VERIFYING LOHÖFER'S EQUATIONS TO ENHANCE ELECTRODYNAMIC SORTING

by

Jaclyn Diane Ray

A thesis submitted to the faculty of
The University of Utah
in partial fulfillment of the requirements for the degree of

Master of Science

Department of Metallurgical Engineering

The University of Utah

December 2016

The University of Utah Graduate School

STATEMENT OF THESIS APPROVAL

The thesis of **Jaclyn Diane Ray**

has been approved by the following supervisory committee members:

Raj Rajamani ,	Chair(s)	**17 October 2016** Date Approved
John Matthews ,	Member	**3 October 2016** Date Approved
Swomitra Mohanty ,	Member	**3 October 2016** Date Approved

by **Manoranjan Misra** , Chair/Dean of

the Department/College/School of **Metallurgical Engineering**

and by **David B. Kieda** , Dean of The Graduate School.

ABSTRACT

Despite the fact that scrap metal recycling is a profitable industry, there are limitations to the methods currently being used to sort the scrap. Particle sizes below 2.5 cm present the biggest challenge for current sorting technologies. This limitation creates a need for an improved technique to sort scrap metal. Electrodynamic Sorting, which uses stationary magnets with a time-varying magnetic field, is investigated as a tool that can overcome these limitations within the scope of this paper. The objective of this thesis is to provide insight into the properties governing Electrodynamic Sorting.

This thesis explores the relationship between power and frequency for two different kinds of magnets. The end results show that the magnets, which are made of different materials, both had a parabolic fit when power was plotted against current as well as when power was plotted against frequency. Another contribution from this work is a comparison of force predictions determined mathematically and the force measured experimentally. With current held constant while frequency was varied, the ejection force on a particle placed within a gapped toroid magnet was measured and plotted against a mathematically predicted plot. The results of the measurements agree with the predicted plot for various size, shape, and types of nonferrous materials used. This information allows us to make some inferences about this Electrodynamic Sorting technique and its potential use in industry.

CONTENTS

LIST OF FIGURES

ACKNOWLEDGEMENTS

I would like to express my gratitude and appreciation to the following individuals:

Dr. Raj Rajamani, for funding my graduate program, offering me a place in his lab, and for pushing my limits, which showed me that the limits I imposed on myself were less than my true capabilities.

Dr. James Nagel, for sharing with me his knowledge and time, and for patiently putting up with too many questions as I navigated through graduate school and this thesis.

Dave Cohrs, for helping set up all of my experimental apparatuses, keeping my work space safe, and always taking the time to answer as well as help me understand my questions.

Jake Salgado, for designing so many items needed to collect my data and all the shenanigans that brought a smile to my face every day.

Dawn Sweeney, for her helpfulness, kindness, and companionship in our lab.

I would like to extend my thanks to Lynnette Moore who offered guidance, friendship, encouragement, and unconditional support during my academic career.

Most of all, I wish to thank my daughter Jenasee Lakey and my son Kyle Lakey, for their patience and understanding during my time away from home so I could pursue my education.

CHAPTER 1

INTRODUCTION

In the United States, metal encompasses nearly every aspect of an average individual's life. Transportation, electronic devices, even the zippers in clothes all contain metal. Other countries working to improve their citizens' quality of lives will notice that their consumption of metals is increasing (Rudenno, 2012). While this demand motivates mining companies to increase the extraction of ore, mines have finite resources and the lifespan of a mine depends on the amount of material inside it and the rate at which it is extracted.

The placement and construction of new mines are dependent on the location of mineral reserves. In many cases, this leads mining companies to remote areas of the world. Although some governments across the planet have federal regulations and standards to protect the environment in which these mines are built, the regulations are practical enough to allow these mines to produce a certain degree of pollution.

Mineral processing visibly affects the land, water, and air while consuming large amounts of power and water. For each one ton of ore milled, the water consumption is 0.8–1.2 kl, the carbon dioxide released is 50–150 kg, and the sulfur dioxide released is 0.1–0.7 kg (Rudenno, 2012). This creates a heavy environmental toll that is not entirely necessary. It is possible to meet many of the demands for metal through the recycling of the scrap metal waste abundant in our society. According to the Institute of Scrap Recycling Industries (Institute of Scrap Recycling, 2016), in 2014 the amount of processed scrap metal in the United States reached, in metric tons, 73 million iron and steel, 5.3 million aluminum, 1.8 million copper, and 250 thousand zinc, to name a few.

Scrap metal recycling has become a high-value industry with the benefit of reducing the pollution caused by primary production. Metals recycling relies on a variety of sorting methods, with eddy current separation being the most widely used. Eriez Magnetics patented its first Eddy Current Separator in 1969 (Benson and Falconer, 1969); however,

to date, conventional machines struggle to sort particle sizes below 25 mm and with little to no specificity between alloys.

Complications lie in the design of the machines. Eddy Current Separation works by inducing eddy currents in nonferrous materials. To do this, bulk material is first passed through a shredder to make a manageable particle size. Next, the particles are placed on a conveyor belt and transported to a rotating magnet, with fixed alternating north and south poles. The arrangement of these poles produces the time-varying magnetic field needed to induce eddy currents in electrically conductive materials, which are not magnetic.

As differing materials have differing conductivities, a range of eddy currents are produced in a collection of scrap metal. When a paramagnetic material enters a time-varying magnetic field with a gradient, eddy current is induced, producing a torque on the particle. In the magnetic field, the gradient produces asymmetric forces on the particle. The torque is responsible for the separation mechanism. Differing conductivities between materials create differing forces on the particles. By placing bins at various distances from the rotor, materials with differing conductivity are separated by the magnet.

Nugget shaped particles below 1.0 cm, small pancake shaped pieces of metal, and shredded wire do not have sufficient mass to produce enough eddy current to be separated by conventional eddy current sorters. A solution to the problem of sorting-limitations was developed by the University of Utah under a grant provided by the Department of Energy. The solution comes in the form of Electrodynamic Sorting (EDX). A fundamental difference between the currently employed techniques and the EDX technique is how the magnetic field is generated.

Whereas traditional techniques use rotating magnets, EDX uses no moving parts; instead, it uses a stationary electromagnet, enabling EDX to reach higher frequencies than conventional sorters. The frequency from a multipolar magnet, like the one Eriez Magnetics uses, is related to the rotational speed of the rotor and the number of poles. Rotational speed is limited by mechanical stress and by rotor strain, which puts limits on the available frequency. For example, a rotor that spins at 100 revolutions per second with 16 magnetic poles can produce a frequency of 1600 Hz.

In contrast, EDX has been demonstrated at 43,000 Hz. Frequency and magnetic field determine the force exerted on particles, which in turn determines the ejection parameters.

To optimize sorting abilities, this information is crucial. A method of feeding the material into the EDX magnetic field is evolving in order to deal with the pancake and wire shaped materials that are typically found in scrap metal waste streams.

This thesis seeks to improve our understanding of the fundamental physics of EDX by introducing the reader to Maxwell's equations and by following first a simplified example and then a more complicated one. Another contribution of this thesis is the exploration of the amount of power consumed by magnets that could be used in industry. Two u-shaped magnets, one made of electrical steel and the other of manganese zinc, are used to explore the relationship between power and current as well as the relationship between power and frequency. The final contribution of this work is a comparison between a predictive model and real-life measurements of force from particles of various size, shape, and conductivity, which are placed in a gapped toroid magnet with a time-varying magnetic field. This is done to see if a model could be applied to the real world.

1.1 Summary Outline

This thesis is organized as follows:

Chapter 2, *Physics of Electrodynamic Sorting*, provides a basic mathematical introduction to electromagnetic equations used to optimize eddy current separation techniques. It also introduces the reader to the most important physics concepts such as Maxwell's equations and Lorentz force, which are used throughout this thesis and in the scientific literature to solve various problems.

Chapter 3, *Power Consumption*, explores the relationship of power and current and the relationship of power and frequency by introducing the reader to an experimental setup designed to vary frequency and current to determine power loss.

Chapter 4, *Electrodynamic Force*, explores the effects that varying current and then varying frequency have on the force impressed upon a particle within a time-varying magnetic field.

Chapter 5, *Conclusion*, reviews the findings of this thesis and discusses opportunities for future developments.

CHAPTER 2

PHYSICS OF ELECTRODYNAMIC SORTING

The physics behind EDX technology has been around since Faraday (followed by Maxwell and Lorentz) investigated electromagnetic properties. Their scientific contributions led to Edison's discovery and patent in 1880 (Edison, 1890) of a device that could separate magnetic ore from nonmagnetic raw materials. This understanding of magnetic induction is still used today by the scrap metal recycling industries. Industrial scrap metal is recycled by the use of a permanent magnet's magnetic field to induce a magnetic force on a conducting particle that enters said field, causing the electrons within the particle to excite. This is known as eddy current.

For this technique to work, there must be an alternating magnetic field. This field is typically created for industrial purposes by rotating a drum with alternating north- and south-pole magnets attached together, rotating it rapidly as a conveyor belt carries particles into the magnetic field, as shown in Figure 2.1. The more conductive the material is, the stronger force it experiences as the induced eddy currents try to oppose the external magnetic field. With a high degree of force, the particles can be separated based on their size, shape, and conductivity by placing a barrier between the trajectories of the different materials coming off of the conveyor belt.

Although the current system works and separates metals, it also has some serious limitations. It is currently difficult for industrial recycling facilities to sort particles below 1.0 cm. The industrial sorting system design produces limitations on the size of the particles that can be sorted. There is a maximum rotation that can be used with these drums, limiting the frequency response. Rotation of the drums also causes wear and tear on the system.

In contrast, the EDX technique used in this thesis seeks to eliminate the mechanically and electrically intensive elements by avoiding a rotary drum and using steady-state magnets

instead. This idea is developed from a patent written by Saveliev (Saveliev, 1998), which passes an alternating electric current through a toroid-shaped nonferrous magnet from which a time-varying magnetic field radiates. A gap with a particular geometry is cut into the toroid so as to produce a magnetic field with a gradient. This gradient is needed for the torque it produces on the conductive particles entering the gap. Certain elements of the original EDX design are evolved from Saveliev.

This thesis finds that the EDX technique can produce the same separation abilities as industry; however, it comes with a unique property. The alternating current around the toroid can be tuned by adjusting the magnet frequency. This in turn affects the force acting on the particles. As such, smaller particles (less than 1.0 cm) that can only be moved by a higher frequency can then be sorted, as can alloys, whose conductivities are too similar for industrial methods to distinguish between them.

For industrial machines to reach the same frequency as the steady state magnets, the rotational acceleration of the drum's rotor must increase. Alternatively, industry could increase the number of north- and south-pole magnets on the drum to reach an equivalent frequency, but this increase lowers their magnet field strength due to the decrease in the size of each magnet. This limitation alone makes EDX a better candidate for industrial scrap metal sorting. The goal of this chapter is to acquaint the reader with the most important physics behind EDX technology.

2.1 Maxwell's Equations

The theoretical foundations of EDX encapsulates Maxwell's equations. This section reveals Maxwell's equations and their significance in EDX technology. Starting with Faraday's law (Jackson, 1998, page 238), we see that a time varying magnetic field gives rise to an electric field

$$\nabla \times \mathbf{E} = -\frac{\partial \mathbf{B}}{\partial t} \ . \tag{2.1}$$

Another equally important equation from Maxwell is that electric currents give rise to a magnetic field

$$\nabla \times \mathbf{B} = \mu_0 \mathbf{J} + \mu_0 \epsilon_0 \frac{\partial \mathbf{E}}{\partial t} \ . \tag{2.2}$$

This equation indicates that an electric field is induced when there is a changing magnetic field. Where μ_0 is the permeability of free space ($4\pi \times 10^{-7}\,\mathrm{N/A^2}$) and ϵ_0 is the permittivity

of free space ($8.854 \times 10^{-12}\mathrm{F} \cdot \mathrm{m}^{-1}\mathrm{S}$). For convenience, these equations can be written in phasor notation, where $d/dt = -j\omega$,

$$\nabla \times \mathbf{E} = j\omega\mathbf{B} \ . \tag{2.3}$$

$$\nabla \times \mathbf{B} = \mu_0\mathbf{J} + j\omega\mu_0\epsilon_0\mathbf{E} \ . \tag{2.4}$$

Since we are only concerned with operations that use such low frequencies, the quasi-static approximation is applied. This states that ω approaches, but does not reach, zero. This reduces Maxwell's equations to

$$\nabla \times \mathbf{E} = j\omega\mathbf{B} \tag{2.5}$$

$$\nabla \times \mathbf{B} = \mu_0\mathbf{J} \ . \tag{2.6}$$

Using Ohm's law, we relate the electric field $\mathbf{E}$ with the current density $\mathbf{J}$ by

$$\mathbf{J} = \sigma\mathbf{E} \ . \tag{2.7}$$

This allows us to express the equation 2.6 as

$$\nabla \times \mathbf{B} = \mu_0\sigma\mathbf{E} \ . \tag{2.8}$$

The application of the cross product to both sides of equation 2.8 leads to

$$\nabla \times (\nabla \times \mathbf{B}) = \nabla \times (\mu_0\sigma\mathbf{E}) \ . \tag{2.9}$$

This equation resembles a well-known identity that states that the curl of a curl equals the gradient of divergence minus the Laplacian. The left side of equation 2.9 thus becomes

$$\nabla \times (\nabla \times \mathbf{B}) = \nabla(\nabla \cdot \mathbf{B}) - \nabla^2\mathbf{B} \ . \tag{2.10}$$

However, we know from Gauss's law that $\nabla \cdot \mathbf{B} = 0$, therefore giving us

$$\nabla \times (\nabla \times \mathbf{B}) = -\nabla^2\mathbf{B} \ . \tag{2.11}$$

By taking the curl of the right side of equation 2.9, we end up with

$$\nabla \times (\mu_0\sigma\mathbf{E}) = \mu_0\sigma(\nabla \times \mathbf{E}) \ . \tag{2.12}$$

We also know, from Maxwell's equations, that $\nabla \times \mathbf{E} = j\omega\mathbf{B}$, which gives

$$\mu_0\sigma(\nabla \times \mathbf{E}) = j\omega\mu_0\sigma\mathbf{B} \ . \tag{2.13}$$

The combined result is

$$-\nabla^2\mathbf{B} = j\omega\mu_0\sigma\mathbf{B} \ . \tag{2.14}$$

The total magnetic field $\mathbf{B}$ is composed of two fields; $\mathbf{B}_e$, which is created be the eddy currents' opposition to the applied magnetic field $\mathbf{B}_i$, giving us

$$\mathbf{B} = \mathbf{B}_e + \mathbf{B}_i \ . \tag{2.15}$$

By putting this result into equation 2.14, we arrive at

$$-\nabla^2\mathbf{B}_e = j\omega\mu_0\sigma\mathbf{B}_e + j\omega\mu_0\sigma\mathbf{B}_i \ . \tag{2.16}$$

After some rearranging and letting $k^2 = j\omega\mu_0\sigma$, we get

$$\nabla^2\mathbf{B}_e + k^2\mathbf{B}_e = -k^2\mathbf{B}_i \ . \tag{2.17}$$

Equation 2.17 resembles the vector Helmholtz equation, which discloses the eddy currents resulting from an applied magnetic field, when given a conductive particle. This formula allows the calculation of net forces and torques for many interesting problems.

2.2 Force on a Square Wire Loop with Inductance

To get acquainted with the process used to solve a problem requiring net force, we begin with a current-carrying wire loop that produces an electromotive (self-inductance). This wire loop, with four equal sides of length L, is placed into a magnetic field with a gradient $\mathbf{B} = (B_0 + \alpha\, y)\cos(\omega t)\hat{z}$. We calculate flux

$$\Phi = \int_{-L/2}^{L/2}\int_{-L/2}^{L/2} (B_0 + \alpha\, y)\ \cos(\omega t)\hat{z}\cdot\hat{z}\, dx\, dy \tag{2.18}$$

$$\Phi = (B_0\, L^2)\ \cos(\omega t). \tag{2.19}$$

Take the time-derivative to solve for ΔV,

$$\frac{-d\Phi}{dt} = \omega\, B_0\, L^2\ \sin(\omega t) = \Delta V. \tag{2.20}$$

The current in the wire now satisfies

$$I = \frac{\Delta V}{Z}\,, \tag{2.21}$$

where $Z = R + j\omega L$. The resistance satisfies $R = \frac{4L}{\sigma\pi a^2}$.

The inductance for a square loop is given as

$$L \cong \frac{2\mu_0 L}{\pi}[\ln(\frac{L}{a}) - 0.774] \tag{2.22}$$

To avoid confusion between inductance and wire length, let length $= W$. The total resistance is now calculated by

$$R + j\omega L = \frac{4W}{\sigma\pi a^2} + \frac{j\omega 2\mu_0 W}{\pi}[\ln(\frac{L}{a}) - 0.774] \ . \tag{2.23}$$

To test this equation, it is assumed that a=0.5 mm and W=1.0 cm. The loop is excited to f=10 kHz, assuming also that the wire is made of copper giving us σ=60 MS/m. The impedance is then

$$Z = (0.85 + 1.12j)\,\mathrm{m}\Omega \tag{2.24}$$

$$\frac{1}{Z} = (4.31 - j5.68) \times 10^2\, S \tag{2.25}$$

$$I = \frac{1}{2}\Delta V = \frac{\omega B_0 W^2}{Z}\sin(\omega t). \tag{2.26}$$

Now the net force is calculated as

$$\mathbf{F} = \int_{\frac{-L}{2}}^{\frac{L}{2}} I\, d\mathbf{l} \times \mathbf{B} = \sum_{i=1}^{4} \mathbf{F}_i \ . \tag{2.27}$$

With some insight, we know that $\mathbf{F}_1 = -\mathbf{F}_3$, which add to cancel each other out. This leaves us with $\mathbf{F} = \mathbf{F}_2 + \mathbf{F}_4$.

$$\mathbf{F}_2 = \int_{\frac{-W}{2}}^{\frac{W}{2}} -I(dx\,\hat{x}) \times (B_0 + \alpha(\frac{-W}{2}))\cos(\omega t)\,\hat{z} \ . \tag{2.28}$$

To keep consistent with phasor notation, let $\mathbf{B}(\mathbf{r}) = (B_0 + \alpha\, y)\hat{z}$. The electromotive force is then

$$\Delta V = \frac{-dI}{dt} = j\omega\Phi = j\omega B_0 W^2 \tag{2.29}$$

where $\frac{d}{dt} = -j\omega$. Thus,

$$I = \frac{j\omega B_0 W^2}{Z} \ . \tag{2.30}$$

This result is plugged into the force equation, giving us

$$\mathbf{F}_2 = -I(B_0 + \alpha(\frac{-W}{2}))W(-\hat{y}) \tag{2.31}$$

$$\mathbf{F}_2 = (\frac{I\alpha W^2}{2} - IB_0W)(-\hat{y}) \ . \tag{2.32}$$

Solving for $\mathbf{F}_4$

$$\mathbf{F}_4 = \int_{\frac{-W}{2}}^{\frac{W}{2}} +I(dx\,\hat{x}) \times (B_0 + \frac{\alpha W}{2})\hat{z} \tag{2.33}$$

$$\mathbf{F}_4 = (I\,B_0W + \frac{I\alpha W^2}{2})(-\hat{y}) \ . \tag{2.34}$$

Adding together

$$\mathbf{F}_2 + \mathbf{F}_4 = -\hat{y}I\alpha W^2 \ . \tag{2.35}$$

The time domain expression is then

$$\mathbf{F}_{net} = \hat{y}\,I_0\,\cos(\omega t + \phi)\alpha_0\,\cos(\omega t)W \tag{2.36}$$

and taking the time-averaged force, the following equation is obtained

$$\mathbf{F}_{avg} = \frac{1}{2}W\,I_0\,\alpha_0\,\cos(\phi)\,\hat{y} \ . \tag{2.37}$$

Please note the magnetic field gradient and the self-inductance L. The gradient provides a net force but not an average force. Everything sums to zero in the absence of inductance. The addition of the self-inductance creates the phase delay, which gives the average force. Thus, it is the magnetic field gradient in combination with self-inductance in the loop that gives a non-zero force.

2.3 Lohöfer's Equation

Though the derivation presented in section 2.2 is long, it is not very complicated. This is due to the fact it is a two-dimensional problem with symmetry, given a cartesian coordinate system. A more complicated problem, involving a magnetically levitated conducting sphere, was solved in 1964 by Peter Rony (Rony, 1964) who was working for the Lawrence Radiation Laboratory in Berkeley California at the time.

G. Lohöfer took Rony's methods one step further when, in 1989, he investigated the absorbed power from electromagnetically levitated metal spheres (Lohöfer, 1989). This thesis uses Lohöfer's equations to predict the force acting on particles placed in an alternating magnetic field. Since Lohöfer's equations are fundamental to the work presented in this

thesis, an explanation of his derivations is presented in this section to give the reader some insight into how the physics is applied.

Given an impressed magnetic field $\mathbf{B}_i = B_0\hat{z}$, the vector potential in spherical coordinates is calculated by $\mathbf{B}_i = \nabla \times \mathbf{A}_i$. Rony guessed the solution in his paper to be

$$\mathbf{A}_i(r,\theta,\phi) = \frac{1}{2}B_0\, r\sin(\theta)\hat{\boldsymbol{\phi}}\ . \tag{2.38}$$

We know that $\mathbf{A} = A_r\hat{\boldsymbol{r}} + A_\theta\hat{\boldsymbol{\theta}} + A_\phi\hat{\boldsymbol{\phi}}$ (Nagel, 2016). However, $\mathbf{A}$ is only excited along the ϕ direction, thus $A_r = A_\theta = 0$ and $A_\phi = \frac{1}{2}B_0\, r\sin(\theta)$. We also exploit symmetry around ϕ, which gives us $\frac{\partial}{\partial\phi} = 0$. Starting with the Laplacian $\nabla^2\mathbf{A}$ from Helmholtz equation 2.17 find

$$\nabla^2\mathbf{A} = [\nabla^2\mathbf{A}_\phi - \frac{A_\phi}{r^2\sin^2(\theta)}]\hat{\boldsymbol{\phi}}\ . \tag{2.39}$$

After plugging everything in

$$\nabla^2\mathbf{A} - \frac{A_\phi}{r^2\sin^2(\theta)} + k^2\, A_\phi = 0\ . \tag{2.40}$$

Next taking out $\hat{\boldsymbol{\phi}}$, move from a vector Laplacian to a Laplacian operator. In spherical coordinates and knowing that since $A = \frac{1}{2}\sin(\theta)\hat{\boldsymbol{\phi}}$ gives $\frac{\partial A_\phi}{\partial\phi} = 0$, end up with

$$\nabla^2\mathbf{A} = \frac{1}{2}\frac{\partial}{\partial r}[r^2\frac{\partial A_\phi}{\partial r}] + \frac{1}{r^2\sin(\theta)}\frac{\partial}{\partial\theta}[\sin(\theta)\frac{\partial A_\phi}{\partial\theta}] \tag{2.41}$$

Plug the result into the Helmholtz equation

$$\frac{1}{2}\frac{\partial}{\partial r}[r^2\frac{\partial A_\phi}{\partial r}] + \frac{1}{r^2\sin(\theta)}\frac{\partial}{\partial\theta}[\sin(\theta)\frac{\partial A_\phi}{\partial\theta}] - \frac{A_\phi}{r^2\sin(\theta)} + k^2A_\phi = 0\ . \tag{2.42}$$

Notice that it is necessary to take the derivative of two variables, r and θ, therefore the method of separation of variables must be invoked to arrive at $A_\phi(r,\theta) = R(r)\Theta(\theta)$ and it is straightforward to show

$$r^2\frac{R''}{R} + 2r\frac{R'}{R} + k^2r^2 = -\frac{\Theta''}{\Theta} - \frac{\cos(\theta)}{\sin(\theta)}\frac{\Theta'}{\Theta} + \frac{1}{\sin^2(\theta)}\ . \tag{2.43}$$

With some foresight, $n(n+1)$ is used as a constant so that

$$r^2R'' + 2rR' + [k^2r^2 - n(n+1)]R = 0\ , \quad \text{and} \tag{2.44}$$

$$\Theta'' + \frac{\cos(\theta)}{\sin(\theta)}\Theta' + [n(n+1) - \frac{1}{\sin^2(\theta)}]\Theta = 0\ . \tag{2.45}$$

It may not be immediately apparent, but equation 2.44 is the spherical Bessel differential equation with order n. Equation 2.45 is the associated Legendre differential equation also

with degree n with order $m = 1$. Both of these equations have well-known solutions, which are given as

$$R(r) = C_1 J_n(kr) + C_2 Y_n(kr), \quad \text{and} \tag{2.46}$$

$$\Theta(\theta) = D_1 P_n^1(\cos(\theta)) + D_2 Q_n^1(\cos(\theta)) \ , \tag{2.47}$$

where J_n is a Bessel function of the first kind and Y_n is a Bessel functions of the second kind. Likewise, P_n^1 is the associated Legendre function of the first kind and Q_n^1 is the associated Legendre function of the second kind.

For regions outside of the sphere where r ¿ a, recognize that $k = 0$. This changes equation 2.44 into

$$r^2 R'' + 2rR' - n(n+1)R = 0 \ . \tag{2.48}$$

This also has a known solution of the form

$$R(r) = C_3 r^n + C_4 r^{-n-1} \ . \tag{2.49}$$

Now the complete solution for A is written as

$$A_\phi(r,\theta) = [D_1 P_n^1(\cos(\theta)) + D_2 Q_n^1(\cos(\theta))] \begin{cases} C_1 J_n(kr) + C_2 Y_n(kr) \ , & (r \le a) \\ C_3 r^n + C_4 r^{-n-1} \ , & (r < a) \end{cases} . \tag{2.50}$$

The next step is to add boundary conditions. The first condition is for a non-zero solution at $r = 0$, but this means that $C_2 = 0$. This is because the second Bessel function, Y_n, is divergent but A_ϕ remains finite. Use also an identity stating $P_1^1(\cos(\theta)) = \sin(\theta)$, leading to $D_1 = 1\, D_2 = 0\, n = 1$ and $C_3 = B_0/2$. By putting these in for equation 2.50, get

$$A_\phi = \begin{cases} C_1 J_1 & (r \le a) \\ \frac{1}{2} B_0 r + C_4 r^{-1} & (r > a) \end{cases} \tag{2.51}$$

The continuity of A across the boundary at $r = a$ results in

$$C_1 J_1(ka) = \frac{1}{2} B_a + C_4 a^{-2} \ . \tag{2.52}$$

When enforcing continuity of the tangential H-fields at $r = a$

$$\frac{\partial}{\partial r}(rA_\phi) \mid_{r=a^-} = \frac{\partial}{\partial r}(rA_\phi) \mid_{r=a^+} \ . \tag{2.53}$$

After performing the calculations to solve for the derivative, find that

$$C_1[kaJ_1'(ka) + J_1(ka)] = B_0 a - C_4 a^{-2} \ . \tag{2.54}$$

Solve for C_1 and C_4 by substitution methods to arrive at

$$C_1 = \frac{3B_0 a}{2kaJ_1'(ka) + 4J_1(ka)} \ , \tag{2.55}$$

$$C_4 = \frac{B_0 a^3}{2}\left[\frac{6J_1(ka)}{4J_1(ka) + 2kaJ_1'(ka)} - 1\right] \tag{2.56}$$

This result is used to solve for the eddy current density noting that $\nabla \cdot \mathbf{A}$=0 and using $\mathbf{J} = -j\omega\sigma\mathbf{A}$. The expression is now

$$\mathbf{J}(r,\theta) = \hat{\boldsymbol{\phi}}\left(\frac{-3j\omega\sigma B_0 a}{2kaJ_1'(ka) + 4J_1(ka)}\right) J_1(kr) s\sin(\theta) \ , \ (r \leq a) \ . \tag{2.57}$$

All that is left to calculate the force is to find the magnetic moment $\mathbf{m}$. As Rony states in his paper, the $C_4 R^2$ looks like a dipole in space. Spherical fields decay like loop fields with a different value for $\mathbf{m}$.

$$\mathbf{m} = \frac{1}{2}\int \hat{r} \times \hat{J} d\tau \tag{2.58}$$

and $\mathbf{r} = r\hat{r}$ with $d\tau = drrd\phi$ thus

$$\mathbf{m} = \frac{1}{2}\int_0^r \int_0^{2\pi} (r\hat{r} \times (J_0 r\hat{\phi} r dr d\theta \tag{2.59}$$

$$\mathbf{m} = \frac{1}{2}\int_0^r \int_0^{2\pi} r^3 J_0 \hat{z} dr d\phi \tag{2.60}$$

finally leading to

$$\mathbf{m} = \frac{r^4 J_0 \pi \hat{z}}{4} \tag{2.61}$$

With the dipole moment $\mathbf{m}$, the following force equation can be solved

$$\mathbf{F} = -\nabla(\mathbf{m} \cdot \mathbf{B}) \ . \tag{2.62}$$

Lohöfer finds that the force on a nonferrous metal sphere is

$$\mathbf{F} = \frac{-\pi R^3}{\mu_0}\mathbf{G}(q)\nabla\mathbf{B}^2 \, , \tag{2.63}$$

where $q = \frac{R}{\delta}$, $\delta = \sqrt{\omega \mu_0 \sigma}$, and

$$\mathbf{G}(q) = 1 - \frac{3}{2q}\frac{\sinh(2q) - \sin(2q)}{\cosh(2q) - \cos(2q)} \ . \tag{2.64}$$

2.4 Discussion

This section provides important insight into the mathematical concepts involved in EDX technology. The wire loop example from section 2.2 sets up an important framework that makes Lohöfer's derivation, in section 2.3, more manageable. With an understanding of the physics concepts involved in EDX, it is now possible to explore how these concepts can help improve sorting techniques. With the aid of Lohöfer and Rony, an equation for calculating eddy currents caused by a time-varying magnetic field is now possible. Chapter 4 of this thesis uses equation 2.63 to calculate the predicted force on a particle placed in a time-varying magnetic field and then compares it to the actual force determined by a force gauge, given identical conditions.

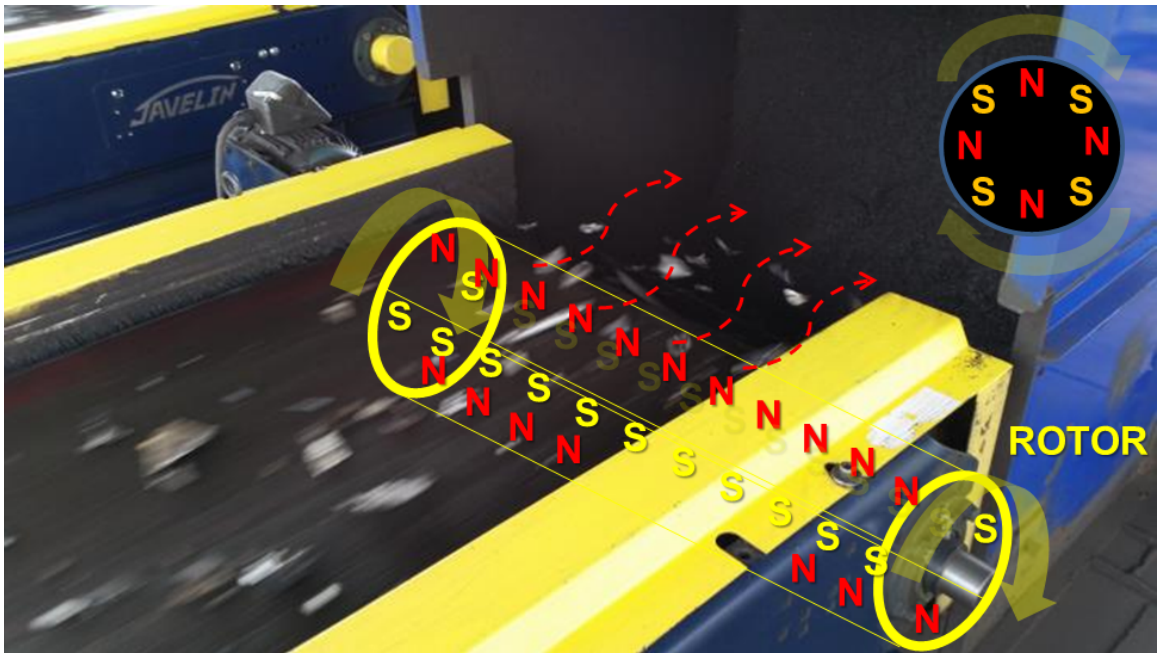

Figure 2.1. A conveyor belt carrying metal and nonmetal pieces of scrap over a rotating drum with alternating north and south pole magnets.

CHAPTER 3

POWER CONSUMPTION

In order to determine which type of electromagnet works best for a given application, it is necessary to understand how much power they dissipate under normal operations. Since average power is an indication of how much electricity is required to sort materials, lower power consumption means a magnet is cheaper to operate. Most power loss is dissipated as heat, which, if left untreated, can cause the magnet to heat up significantly. The insulation from the wires around the magnet may break down if the magnet core itself becomes too hot, resulting in sparks leaping from one wire to another, causing a potential fire hazard.

Heat also lowers the magnetic saturation point, reducing a magnet's performance. Sources of heat can include, but are not limited to, hysteresis loss and eddy current losses. Hysteresis loss is a phenomenon where energy is lost to magnetic materials as they are magnetized and demagnetized. Eddy current loss is also created within a magnetic material, thus producing internal heat.

This chapter explores the behavior of magnetic materials, specifically for two magnets of interest. The research process was done to examine the performance characteristics of the different magnetic materials under conditions of varying current and frequency, separately. The process was as follows: Both magnets were cut as u-shaped cores and had equal physical dimensions. They were wound with Teflon-insulated stranded copper wire with 147 turns per leg of each magnet. When measured with an LCR meter, the inductance read 4.3 mH for both magnets.

The material of the magnets was selected based on their properties. One magnet was made of electrical steel and the other magnet was made of manganese zinc (MnZn). It is important to note here that electrical steel produces a magnetic saturation of up to 2.0 T; it also has a high conductivity of about 10^6 MS/m. In contrast, the MnZn has a lower magnetic saturation of about 600 mT and a lower conductivity of about 10^2 S/m.

The MnZn magnet was made of two solid pieces epoxied together, whereas the electrical steel was made of many thin slabs placed together and secured with screws at the bottom. The slabs were laminated to mitigate eddy currents from within the magnet itself. Figure 3.1 shows front and side images of the electrical steel and MnZn magnets.

Measurements were performed to determine how much power was consumed when operating the magnets. The relationship between power and current was investigated first. Power was measured with frequency held constant at 10.0 kHz while the currents were varied. The relationship of power to frequency was then measured with current held constant at 10.0 A, while the frequency was varied. This was done in order to determine if an increase in frequency would cause a linear increase in power absorption.

3.1 Experimental Setup

The equipment used in the measurements included a signal generator, amplifier, capacitor bank, magnet, current sense resistor, and oscilloscope. Figure 3.2 shows a schematic representation of the experimental setup that was used for both power measurements. Since the electromagnets are large inductors, they are modeled here as an RLC circuit. To prevent field interference between the magnets, they must be located away from one another, as well as the other electrical components. As a result, the magnets were physically separated by about 1.0 m from each other and about 0.5 m from the capacitor banks and wires.

The measurements used CDE Mica capacitors that were special ordered for their current and voltage handling characteristics. Figure 3.3 shows one of the capacitor banks; there were eighteen all together. For the power as a function of current measurements, the capacitance was 60 nF. For the power as a function of frequency measurements, the capacitors needed to be swapped out to obtain the desired frequency.

Since the inductance was fixed, a capacitance able to drive the frequency at resonance was used; at resonance, the capacitive and inductive reactances equaled zero. The capacitance values were determined by the following resonance frequency equation

$$f = \frac{1}{2\pi\sqrt{LC}} \ , \tag{3.1}$$

where C is the capacitance and L is the measured inductance. Solving for C

$$C = \frac{1}{4\pi^2 f^2 L} \ . \tag{3.2}$$

The capacitor values were adjusted until the desired frequency output was reached and the corresponding capacitor value was recorded.

The signal generator was used to set the frequency and send a voltage signal to the amplifier, which has a gain of 20 V/V. As a safety measure, an over-current switch was placed in series with the amplifier to protect it from delivering too much current in the event of a short. Two test-points were used to monitor the circuit. The first test-point was used to measure the amplifier voltage and was placed after the safety switch. The second test-point was used to monitor the signal voltage through a 1.0 Ω resistor. The resistor being 1.0 Ω led to a direct measurement of the current through the resistor, but as a function of voltage and not as a function of amperes. For example, an input current of 1.0 A would produce a voltage of 1.0 V given a resistance of 1.0 Ω.

3.2 Power versus Current

Frequency was held constant at 10 kHz with a capacitance of 60 nF for the power as a function of current measurement. The capacitance was calculated by equation 3.2 with f =10 kHz. As such, the capacitors did not need to be switched out. Since frequency was also at resonance, this implied zero reactance. With no reactance in the circuit, there would be no phase offset.

Beginning with 1.0 A and increasing in 1.0 A increments, up to 20 A, the voltage associated with each current measurement was recorded and average power, for a sinusoidal varying current at fixed frequency in resonance, was calculated by

$$P = \frac{1}{2} I_{peak} \, V_{peak} \ . \tag{3.3}$$

Applying Ohm's law, $V = IR$, and substituting in for V, results in

$$P = \frac{1}{2} I^2 \, R \ , \tag{3.4}$$

where R is the sum of the resistance from the coil and the resistance through the 1.0 Ω resistor.

To determine the resistance in the coil, the 1.0 Ω needed to be taken out of the final calculations. This could be done easily because the resistance was constant with current. The resistance in the coil was then calculated by $R_{coil} = \frac{2P}{I^2}$ which came out to be 4.7650 and 0.9316 Ω for the electrical steel and MnZn, respectively.

Figure 3.4 shows power as a function of current for the electrical steel magnet. This result was plotted against equation 3.3. Note that this fit indicates that the electrical steel follows a parabolic path. Similarly, Figure 3.5 shows the MnZn magnet's power plotted as a function of current. The MnZn curve was also plotted against a parabola and it too shows a good fit. As shown by Figure 3.4 and Figure 3.5, as the current increases, so does the power. The electrical steel consumed nearly twice as much power as the MnZn magnet, as a result of the electrical steel's lower resistivity.

3.3 Power versus Frequency

Capacitor banks were used to change the frequencies for the power as a function of frequency measurements, ranging from 62–1440 nF, with 62 nF corresponding with the highest frequency and 1440 nF with the lowest. Each capacitor provided a resonant point at the associated frequency. The frequencies ranged from 1.76–10.0 kHz. For the MnZn magnet, seventeen capacitor banks were used. For the electrical steel magnet, eighteen capacitance banks were used. The resistivity of the electrical steel material was lower than the resistivity of the MnZn, meaning that the voltage reached the oscilloscope's cutoff limit sooner; therefore, an extra capacitor was required.

For each measurement, the current was held constant at 10.0 A peak. The oscilloscope was then paused and a flash drive was used to collect the current and voltage waveform data. The frequency was increased until the next resonance frequency point was reached.

To calculate the power for the frequency measurements, a slightly different approach was needed. Equation 3.3 could not be used due to the uncertainty in the measurements as well as concerns about nonlinearity. Therefore, instantaneous power was calculated by

$$P(t) = I(t)V(t). \tag{3.5}$$

For more accuracy in the measurements, equation 3.5 was integrated to find the mean value of the power function

$$P = \frac{1}{T}\int_0^T I(t)V(t)dt\ . \tag{3.6}$$

Equation 3.6 is true for continuous functions. However, the oscilloscope only took a finite number of samples (n=2500). An equation was produced to calculate the real-time average power for use in MATLAB

$$P_{avg} = \frac{1}{T}\sum_{i=1}^{n} I_i V_i \Delta t \ . \tag{3.7}$$

Compensating for the current-sense resistor, the total resistance was calculated, as in section 3.2, with $R_{total} = \frac{2P_{avg}}{I^2}$, which gave the inductor power, $P = \frac{1}{2}|I|^2 R_L$, where R_L is the total resistance, and then 1.0Ω was subtracted out.

Figures 3.6 and Figure 3.7 show the power as a function of frequency. As evident by the figures, the electrical steel core has an apparently smoother line than that of the MnZn core. Due to the signal to noise ratio at 10 kHz, the electrical steel magnet power reached 500 W while the MnZn core was less than 70 W at that same frequency. The high power measurement of the electrical steel core was due to the eddy current and the resistive losses in the electrical steel. Both figures show a nearly linear trend. The equivalent series resistance increased with frequency, causing more power to be lost in the system.

3.4 Discussion

The goal of this chapter was to compare two types of materials and determine which one had more favorable properties for industrial scrap metal recycling. When both magnets were observed with the frequency held constant while the current was varied, they both produced parabolic paths with a constant resistance. When looking at the power for both of the magnets in the power as a function of current plots, it is immediately apparent that the electrical steel power values are much higher than they are in the MnZn. Comparing power as a function of frequency showed that Electrical steel, once again, had a higher power dissipation than that of MnZn.

The high resistivity of the MnZn magnet is responsible for reducing power dissipation. However, this magnet also has a lower magnetic saturation point. The Electrical steel produced a stronger magnetic field, which indicates it is better suited for lower frequencies. Electrical steel's higher magnetic saturation and lower frequency range could make it a candidate for sorting alloys. Alloys with similar conductivity will need a stronger magnetic field to be separated from one another. MnZn, on the other hand, would be a better candidate for separating small particles below 1.0 cm.

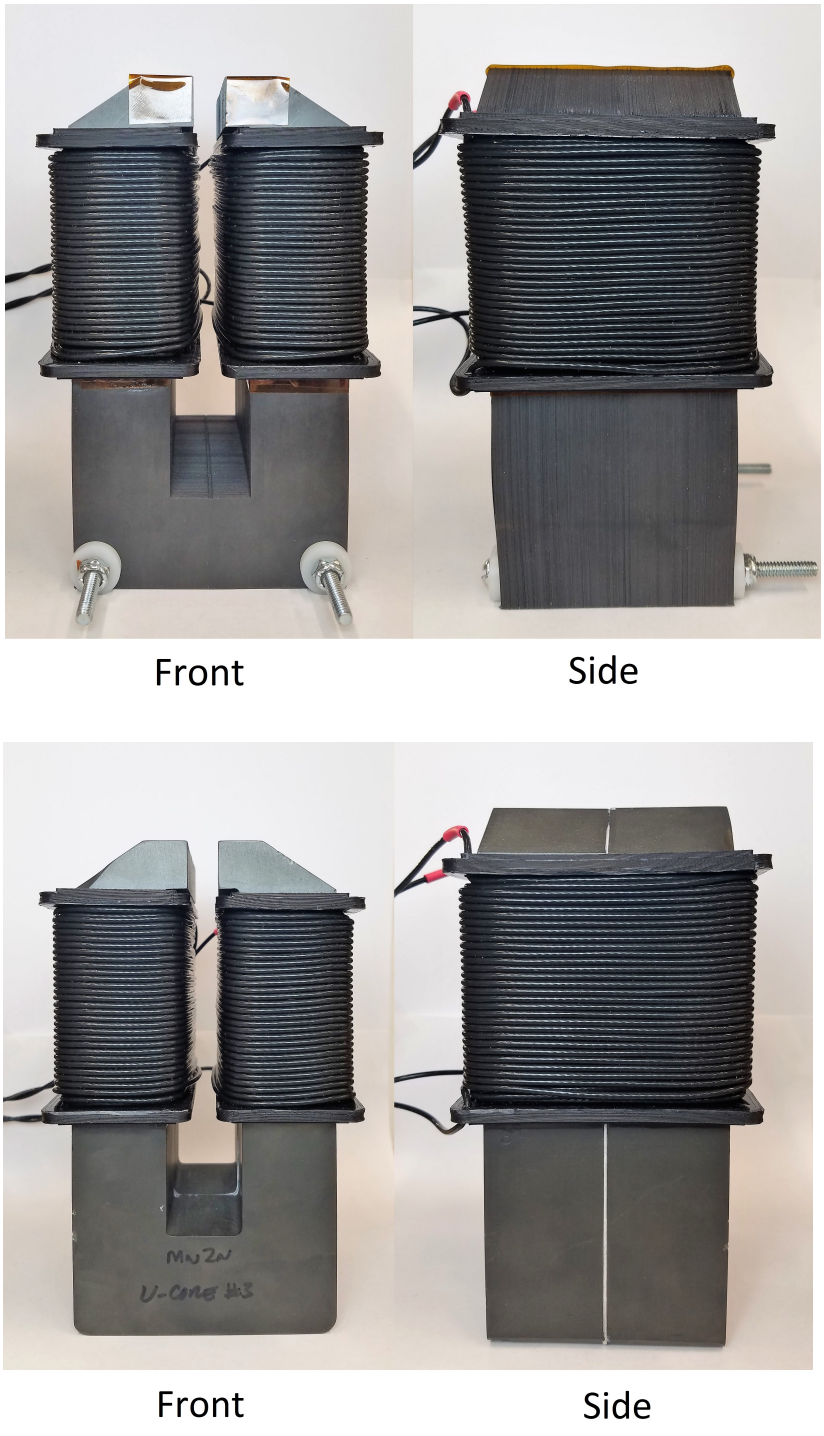

Figure 3.1. Electrical steel magnet (top) MnZn magnet (bottom).

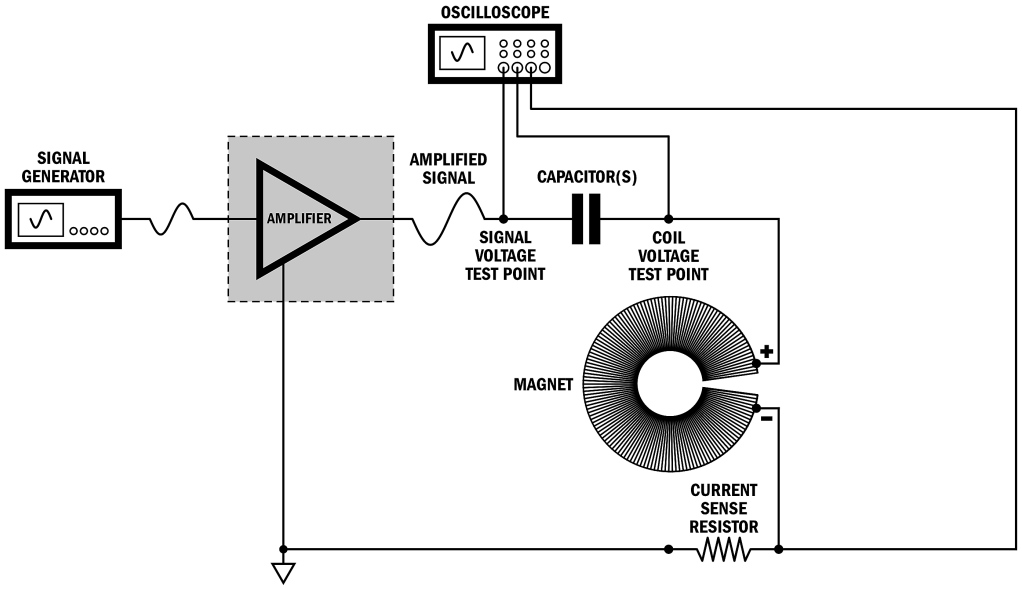

Figure 3.2. Schematic representation of the power measurement setup.

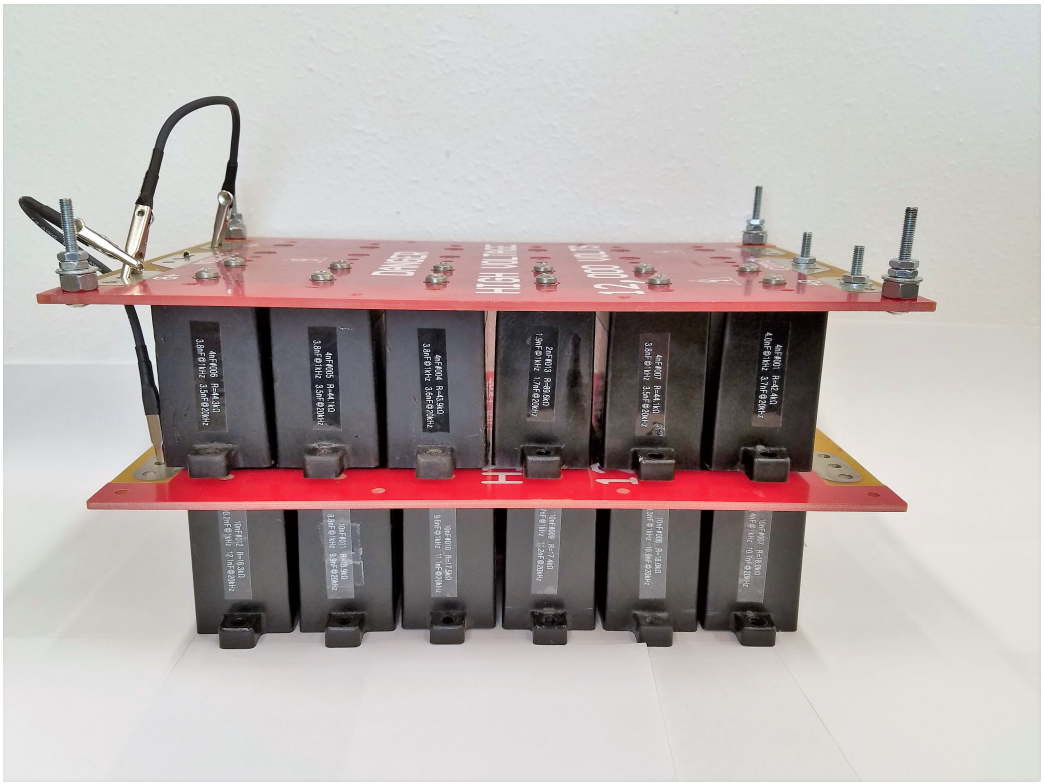

Figure 3.3. Capacitor bank example.

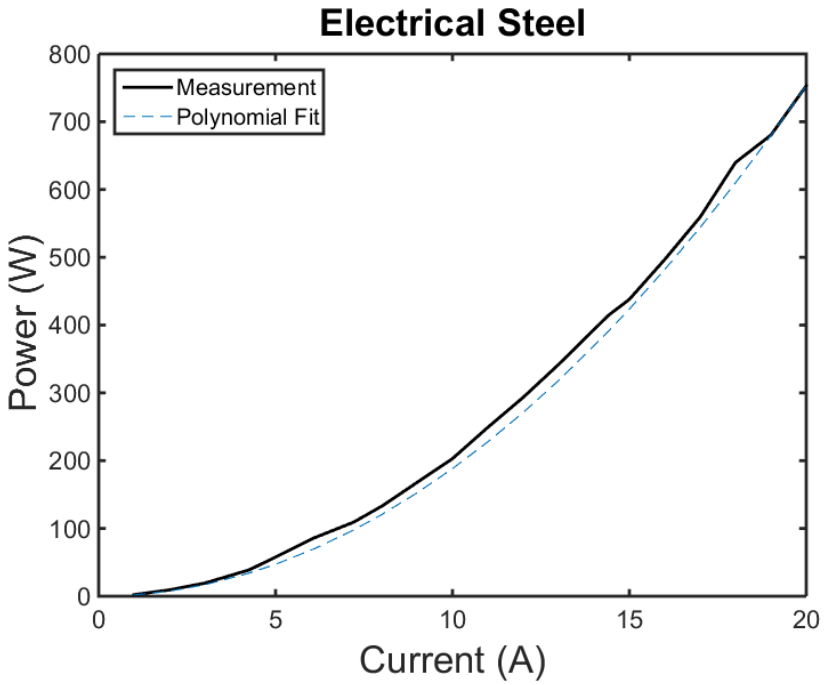

Figure 3.4. Power as a function of current for the electrical steel magnet plotted against equation 3.3.

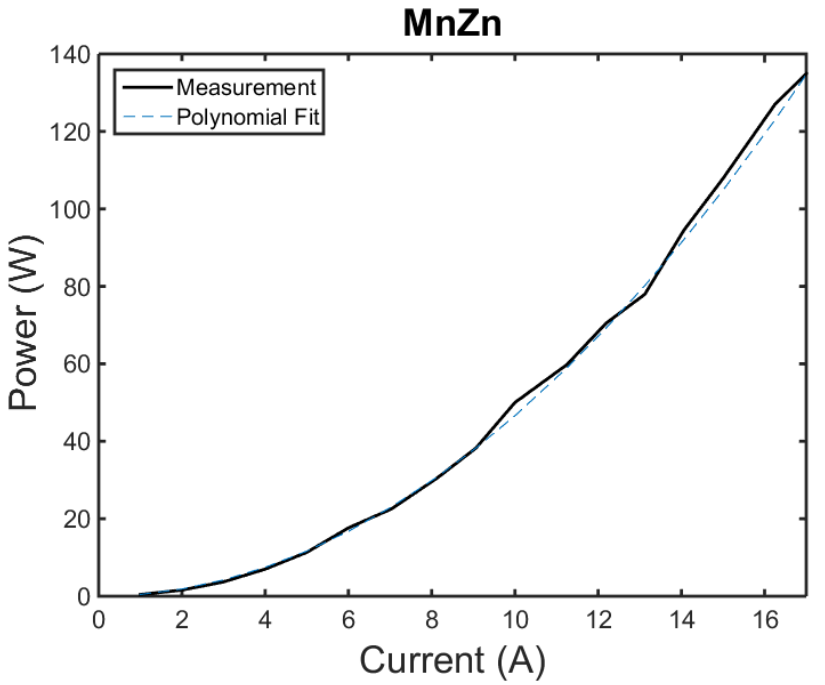

Figure 3.5. Power as a function of current for the MnZn magnet plotted against equation 3.3.

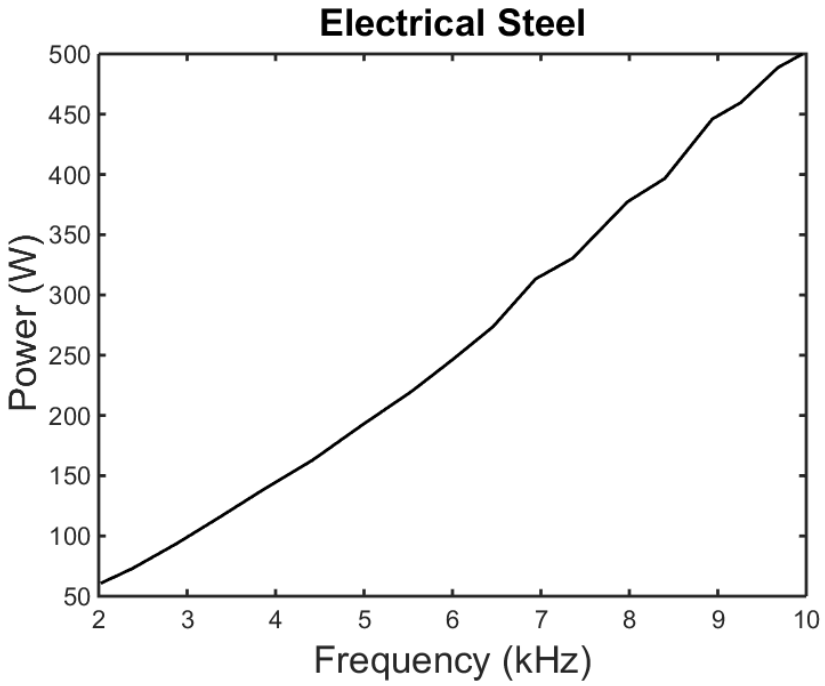

Figure 3.6. Power as a function of frequency for electrical steel magnet.

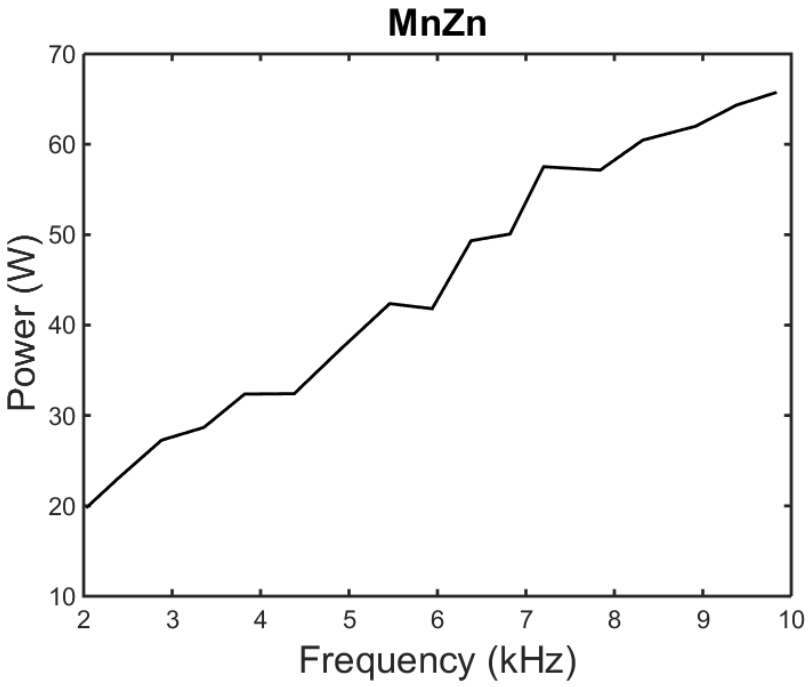

Figure 3.7. Power as a function of frequency for MnZn magnet.

CHAPTER 4

ELECTRODYNAMIC FORCE

The force a particle experiences when it enters an alternating magnetic field will determine how far it is ejected. Ejection is important because it leads to the separation of materials with different conductivities. Conductivity differences between materials will eject some particles farther than others, a characteristic that makes EDX possible. Also, metals of sizes below 1.0 cm can be separated if they experience a great enough force. Currently, these small particles present a challenge to scrap metal recycling industries and the ability to sort such small pieces would increase the industries' profits.

How far a particle is ejected depends on the amount of force the particle experiences as it enters an alternating magnetic field. A theory from Lohofer's equation 2.63 could be used to predict the force the particles will experience in the magnetic field. Solving Lohofer's equation requires the radius of spherical objects and one difficulty that may arrive when using this theory is that most, if not all, of the particles from any given metal recycling industry will not be spherical. Thus, it was necessary to test if the theory would work for various particle shapes.

This chapter discusses the experiments that were conducted to measure how particles behave when placed within the gap of an electromagnet. Section 4.2 discusses the profile of the magnetic field within the gapped toroid magnet. One must understand the magnetic field profile to determine the best location through which to feed scrap material and therefore optimize the accuracy and reproducibility of the sort. This provided the requisite information about the magnetic field strength that will be used as a parameter to test Lohofer's equation.

The relationship between the magnetic field strength and frequency is our primary focus for this chapter. Section 4.3 explores force as a function of frequency measurements that were taken to determine how variously shaped nonferrous particles would respond to an

induced magnetic field. The frequency measurements were then compared to the expected force derived from Lohofer's equation, with the end result being that they agreed very well.

4.1 Experimental Setup

Much of the experimental setup in this section resembles that of section 3.3 measurements with the addition of a Mark-10 model M4-012 digital force gauge, and a Lake Shore Instruments model 475 DSP Gauss meter and probe. The magnet was a 360 mm toroid made from nickel zinc (NiZn). The gap geometry of the NiZn magnet used for this experiment was chosen because of the need for a magnet field with a gradient. The gradient induced a torque on particles as they entered the gap. Also, the magnet was wound with the same 18 gauge Teflon insulated stranded copper wire as the u-shaped magnets. The inductance was measured to be 8.9 mH. The entire apparatus was secured to a wooden frame to minimize movement of components and ensure reproducibility. Figure 4.1 represents a schematic of the design.

The force versus frequency measurements, discussed in section 4.3, also used spherical, cylindrical, disk, and cube samples of aluminum alloys, copper, brass, and magnesium of various sizes. To determine the exact composition, an XRF analyzer was used on all samples before the final plots were made. A Sigmascope SMP10 electronic conductivity meter was used to obtain the conductivity of the samples.

In some cases, the reading from the conductivity meter did not agree with the value from the data sheet that came with some of the particles. The conductivity meter often had difficulties with spheres, even when curvature correction was applied, but it worked great when given a flat surface to analyze. The conductivity meter also incorrectly read the aluminum alloy samples. For many of these samples, it was decided that the value taken from a material data sheet would be used, though not all of the particle samples, such as the copper spheres, had a data sheet.

Because repetitive measurements were taken and the magnet was driven to near saturation, the core tended to heat up over time. This shifted the inductance and reduced the magnetic saturation point as time went on. An ice pack was placed on the core to cool it before further measurements were taken. This had to be done several times to keep the magnet at a stable temperature.

To validate a random sample of each material and size used to represent that sample's population, three 12 mm diameter aluminum 6061 spheres were selected at random (n = 215). Each sphere was tested eleven times at 10 kHz for the force exerted on them. The mean and variance were calculated separately and the confidence interval at 95 % was then determined by

$$\bar{x} - z_{\alpha/2}\frac{\sigma}{\sqrt{n}} \leq \mu \leq \bar{x} + z_{\alpha/2}\frac{\sigma}{\sqrt{n}}. \tag{4.1}$$

Based on the sample data, a range of highly plausible values for a mean force is 65.4 ± 0.1 mN.

4.2 Magnetic Field Profile

Frequency, magnetic field strength, size, shape, and conductivity all play a role in the ability to separate materials from one another. In industry, the size and shape of particles can be controlled by passing them through a shredder and then a sieve. Conductivity is an inherent property of a given material, and is temperature dependent. Magnetic field strength can be controlled based on the type of magnetic material and the operating conditions such as current and voltage. This section investigates magnetic field strength of the magnet.

To determine the field profile of the NiZn magnet, the Gauss probe was moved in 1 mm increments through the gap from the edge of inner diameter to just past the edge of the outer diameter at a constant current first and then with an alternating current with frequencies at 6.5 and 11.5 kHz. An investigation of how varying the current affected the magnet field strength was needed. For the following experiments, the Gauss probe was attached to a 3D printed apparatus that would allow it to be moved horizontally through the gap of the magnet or held stationary. The printed fixture had a ruler attached so that the precise location in the field could be determined for any given location.

4.2.1 Magnetic Field versus Position Using Direct Current

The Gauss probe was placed a few millimeters behind the inner ring of the magnet, where the gap was the narrowest and the magnetic field would be the strongest. From there, the probe was then moved in 1 mm increments and the magnetic field at each location was measured and recorded. This measurement was performed using constant current of 7.6 A. The field versus position profile was performed twice to verify that the profile could be

reproduced.

Measurements revealed that the magnetic field was increasing as the probe neared the back of the gap. Once the probe was inside of the gap, the field strength increased to its maximum value and then gradually decayed as the probe moved towards the front of the gap, where the separation distance for the gap was largest. The measurements ended when the probe was just outside of the gap, where field leakage was minimal. Note that the zero point on the position axis does not correspond with the back of the gap. Maximum magnetic field values occurred at the point where the gap was smallest. Figure 4.2 shows the two measurements and how well they agreed. The slight deviation of the two measurements is due to the movement of the Gauss probe.

4.2.2 Magnetic Field versus Position Using Alternating Current

Next, a field profile was taken, this time using alternating current. Three capacitor banks were set up to tune the magnet to 6.5 and 11.5 kHz with the current set at 7.60 A_{peak}. The Gauss probe was again placed past the back of the gap and moved in 1 mm increments while the magnetic field strength at each corresponding location was recorded. Figure 4.3 shows the magnetic field versus position profile for the two frequencies used.

The measured values were multiplied by $\sqrt{2}$ to compensate for the root mean square to convert to peak power because the magnetic field measurements were taken as RMS. The two plots agree very well; however, there is a small discrepancy at the peak magnetic field that was due to the current. Current, as read on the oscilloscope, would occasionally increase during the 6.5 kHz measurements to 8.0 A_{peak}. The slight increase in current would explain the periodic increase in the magnet field values. However, the two plots agreed well enough to show that the magnet field strength does not change, regardless of the frequency, so long as current is kept constant.

4.2.3 Magnetic Field versus Current

Although the field strength was highest at the back of the magnet where the gap was the smallest, it was not feasible to use this location for the experimental work in this thesis. It was decided that the location of the magnetic field probe for all remaining measurements would be where particles would most likely fall during real industrial sorting. Magnets must be gapped according to the size of the particle being sorted.

Using direct current, and keeping the Gauss probe stationary at the 23 mm location from the back of the gap, the current was increased from 2 to 21 A, in 1.0 A increments, and the corresponding force for each current was measured and recorded. The probe was then moved further inward to the 33 mm mark where the separation distance of the gap increased and the measurements were repeated. The results are shown in Figure 4.4. The strength of the field showed an increase with increasing current for both positions, which was to be expected. Due to the width of the magnet at 33 mm being larger, the magnetic field strength was thus weaker than the 23 mm position.

The final measurements in this section were taken using alternating current to see if the magnetic field profile looked the same. The current increased from 1 to 12 A in 1.0 A increments. The frequencies chosen for this measurement were 2, 5, 7, 9, and 10 kHz. The Gauss probe was held stationary between the 23 and 33 mm point. Figure 4.5 shows the magnetic field versus current with frequency held constant for each of the measurements performed. All of the plots show a nearly linear response. The nonlinear transition is due to saturation of the magnetic core material.

4.3 Magnetic Force versus Frequency

With a firm grasp of a magnets relationship between current and frequency, the next step leads to the bulk of this thesis work, where the relationship between force and frequency is explored. Our goal is to determine if Lohofer's equations will predict the force a particle experiences when placed in the magnetic field gradient. To do this, an apparatus was designed to hold individual particle samples within the gap of the magnet. Polyester strings were attached at one end to the apparatus and the other end was wrapped around the particle. Super glue was used to secure the string to the particles, allowing them to be suspended, individually, within the gap of the magnet. The force probe was then positioned so when a particle was ejected from the field the instant the magnet was energized, its impact on the force probe would be measured.

The physical location at the center of the particle, when suspended in the gap, was recorded. The magnetic field intensity needed to be measured at that precise location, which meant that the particle needed to be temporarily removed. Magnetic field strength was measured and recorded at the corresponding location and its value was used as the

magnetic field value in Lohofer's equation.

Since it is the magnetic gradient that induces the particle's ejection from the magnet, this quantity also needed to be determined. Magnetic field strength on either side of the center measurement was recorded at a 1.0 mm distance, so that the gradient of the magnetic field through the particles could be calculated by the following numerical derivative

$$\frac{dB}{dx} = \frac{B_2 - B_1}{x_2 - x_1} \tag{4.2}$$

where B_2 and B_1 are the magnetic field strengths recorded on either side of the center position and x_2 and x_1 are the physical locations within the gap.

Current was then measured with an oscilloscope using the cursor function to place a marker at the top of the current waveform. This step was important because once the Gauss probe was removed and the particle placed back in the gap, the magnetic field will be lower than the previously measured value, due to the particle acting as a flux bridge, which temporarily lowers the inductance of the system. Placing the particle in the gap and tuning the frequency so that the current waveform on the oscilloscope once again matched the cursor from the previous reading ensured that the magnetic field had the same intensity as it did without the particle.

Eddy currents generate heat within the particles while they are in the alternating field, causing the conductivity of the particles to lower. To prevent this from happening, a step was taken in between measurements to submerge the particle samples in an ice water bath for a few seconds to cool them. This kept the samples at nearly the same temperature throughout the measurements.

Five frequencies were used for the measurements in this section; 2, 4, 6, 8, and 10 kHz. Because the inductor voltage increases with increasing frequency, measurements began at 10 kHz. This frequency would set the standard for how hard the magnet could be driven without exceeding the dielectric strength of the coil's wire insulation, or the maximum amplifier supply voltage. Copper spheres measuring 5.56 and 15.01 mm were measured first. Once a sphere was placed within the gap, the magnet was energized, which immediately pushed the sample into the force probe. Using the Measure Lite software supplied with the force gauge, the number of readings was set to 10 and acquisition of the data began.

The procedure was performed twice for each particle at each frequency. The data were

saved to an Excel file and the average force calculated. Force versus frequency was plotted against Lohofer's predicted values. Figure 4.6 shows the force versus frequency for the two copper spheres.

The plots are slightly offset from the predicted line due to the value chosen for the conductivity of the copper. Because these samples did not come with a data sheet, a best estimate of the conductivity was used. The critical observation is that the two spheres follow the predicted plot's form.

Aluminum alloy spheres were tested next. Figure 4.7 shows the plots of aluminum alloy spheres of different diameters. The smaller 5.56 sphere was 2017 aluminum whose measured values agree very well with the Lohofer curve. Aluminum 6061 and 2024 measured values also fit very well with the predicted force. The aluminum 1100 samples measured values varied slightly, however. This is likely due to the magnet core heating up, reducing the magnetic saturation point. Again, this was why it proved important to cool the magnet in between measurements.

Two brass spheres were also tested. One had a diameter of 6.33 mm and the other 19 mm. The value for the conductivity used came from the conductivity meter's reading of a cylindrical brass sample after the XRF analyzer revealed they had the same composition. Figure 4.8 shows the force measurements on the brass spheres. Brass followed the predicted curves very well.

The data from all of the spherical samples fit well with the expected plots generated from Lohofer's equation. Samples that have the correct shape but do not have the same values as the predicted plot indicate the importance of conductivity as a master variable. Using a value for conductivity that is not a true representation of the material used would produce data points that slightly vary from the expected plot.

After the spheres were measured, the next step was to determine how well cylinder samples matched with the expected plot. However, in order to calculate Lohofer's equation, the radius of a sphere is required. A method for calculating an equivalent volume was proposed. Setting the equation for volume of a sphere and volume of a cylinder equal to one another and solving for the radius of the sphere should provide an equivalent radius. The following equations show how the equivalent spherical volume was computed:

$$\frac{4}{3}\pi r_s^3 = \pi r_c^2 h \tag{4.3}$$

$$r_s = \sqrt[3]{\frac{3}{4} r_c^2 h}. \tag{4.4}$$

Once the data were compared using these values, we observed that they did not agree with the expected plot. The radius of a cylinder was overestimated using this method. Further calculations were performed in an attempt to understand why equivalent volume was not working. It was determined that multiplying the equivalent radius by a weighting coefficient of 0.9 would correct for all of the cylindrical samples.

The reason the equivalent volume was not working is due to the difference between the area of a sphere and the area of a cylinder at the back of the gap, where the field strength is preponderant. The cylinder had more area in the back, and so it experienced a stronger force than the sphere, whose curvature minimized its area in the stronger part of the magnetic field, indicating that there does exist an equivalent sphere that can accurately model the behavior of a cylinder.

Figure 4.9 shows the aluminum cylinder force measurements compared with Lohofer's predicted curve. The equivalent radius was used with the weighting coefficient and accurately modeled a 6 and 12.5 mm diameter cylinders.

Figure 4.10 shows the brass cylinder measurements. These cylinders had the same dimensions as the aluminum and the same equivalent spherical radius was used to plot the expected curve. Figure 4.11 illustrates magnetic force as a function of frequency for the copper cylinder samples. Again, the same value of equivalent sphere was used as all the cylindrical samples were cut to the same dimensions. Lohofer's equations proved they were able to accurately predict the force for the cylindrical samples.

The cube and disk samples used a similar method to find equivalent spherical radii needed for Lohofer's equation. Figure 4.12 shows the plots for two aluminum 6061 cubes, one at 5.5 mm and the other 11.4 mm in length. The force values for the larger cube samples were slightly off from the expected plot but the overall shape still agreed. The brass cube force measurements fit even better than the aluminum, given the same size cubes as shown in Figure 4.13. Even the copper cubes followed the predicted curve, as Figure 4.14 shows.

Disks produce interesting results. As a disk responds to an alternating magnetic field, it acted to orient itself in such a way that it approached its lowest energy state. A torque was induced on the disks that makes them difficult to sort. It also prevented the force probe

from getting a stable reading. To take a measurement of the disk samples, a special 3D printed form was attached to the force probe to hold the disk at the desired orientation within the magnetic field and prevent it from rotating.

By holding the disk stationary in the magnetic field, consistent force measurements were obtained. The disk particles heated up more quickly than all previous samples and required more frequent cooling. The excess heating can be understood by considering the thermodynamic $\frac{P}{V}$ relationship between disks and spheres.

Figure 4.15 shows the results for disk samples of aluminum, brass, and copper. The aluminum disk samples experienced the most internal heat; they continually burned the thread that held them in position within the gap. Due to excessive heating, the 2 kHz reading for the aluminum sample could not be taken. The heat from the disk melted the plastic from the 3D printed fixture that held them stationary within the gap. Due to these complications, no further measurements were made.

4.4 Discussion

Lohofer's equation offers a strong prediction of the force imparted on a spherical particle. Though there were some variations within the data presented, the overall fit to the corresponding Lohofer curves was quite satisfactory. Lohofer's equation also worked to predict the force exerted on nonspherically shaped particles.

Since it was established that Lohofer worked to predict a curve for force as a function of frequency, a simulation was produced to show the curves for three types of aluminum alloys. A plot to compare the curves of aluminum, brass, and copper was also simulated. Figure 4.16 shows the two plots. The left plot shows the curves for aluminum alloys 1100, 2024, and 6061. It also shows the plots for aluminum 6061, brass, and copper.

These plots provide information about which frequency, for a given particle size, could be used to sort the materials. Nearly any frequency would sort copper from aluminum, and brass. To separate aluminum from brass, a frequency between 8 and 10 kHz with 100 mT magnetic field would suffice. Based on the experimental data presented, Lohofer's equation is an appropriate formula to determine what frequency is necessary to optimize material sorting in recycling or other applications.

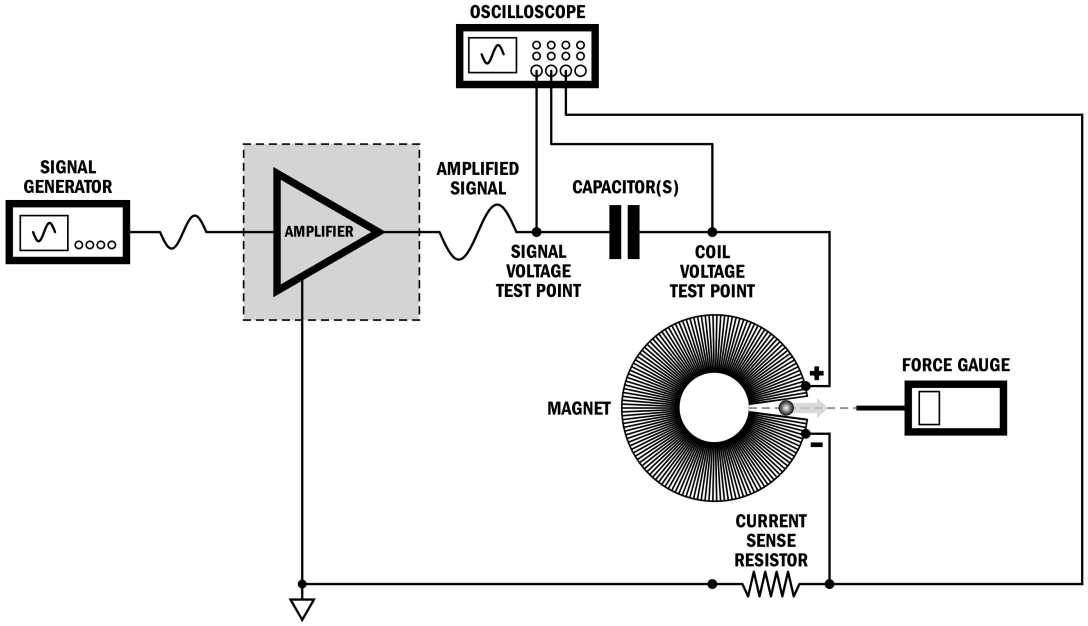

Figure 4.1. A schematic representation of the force measurements setup.

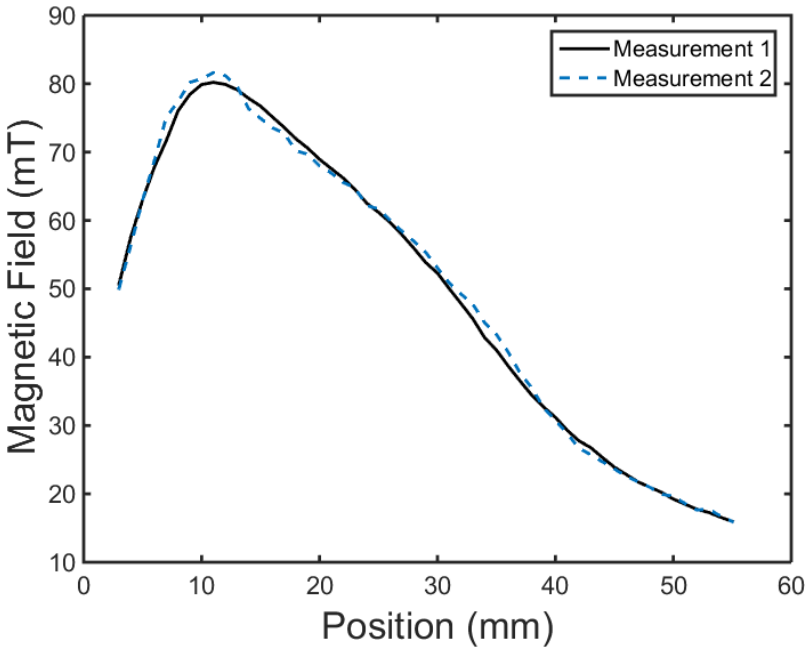

Figure 4.2. Magnetic field versus position for two measurements at DC.

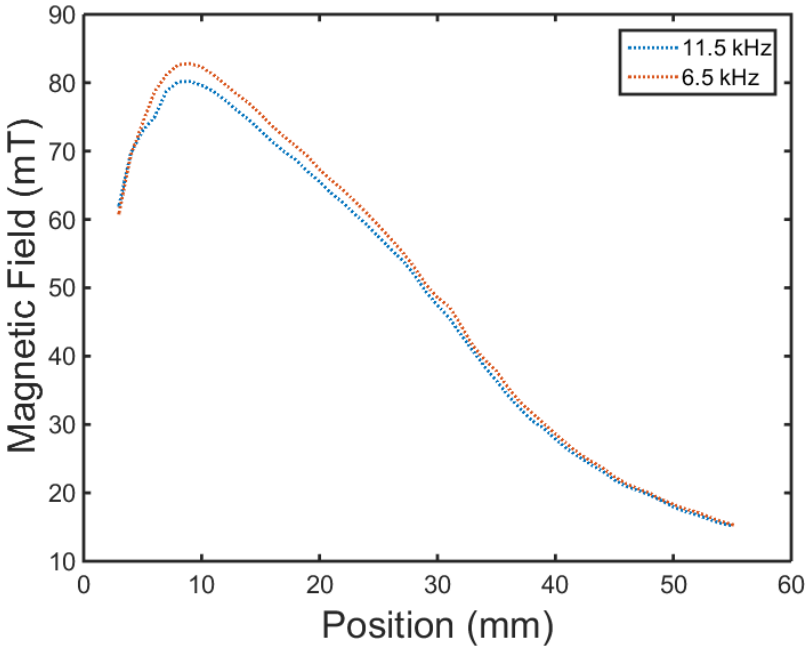

Figure 4.3. Magnetic field versus position for 6.5 and 11.5 kHz frequencies.

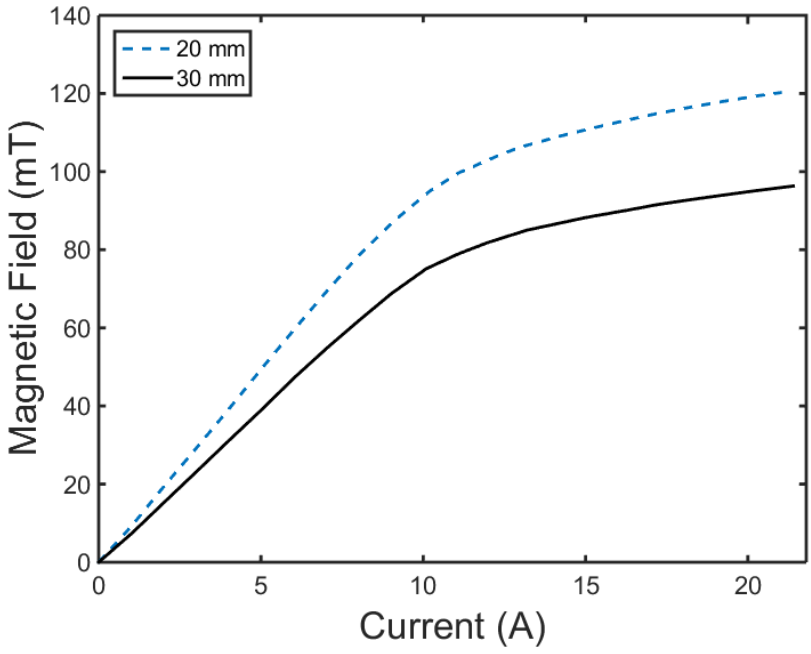

Figure 4.4. Magnetic field versus current as the Gauss probe was held stationary at 23 mm and then 33 mm.

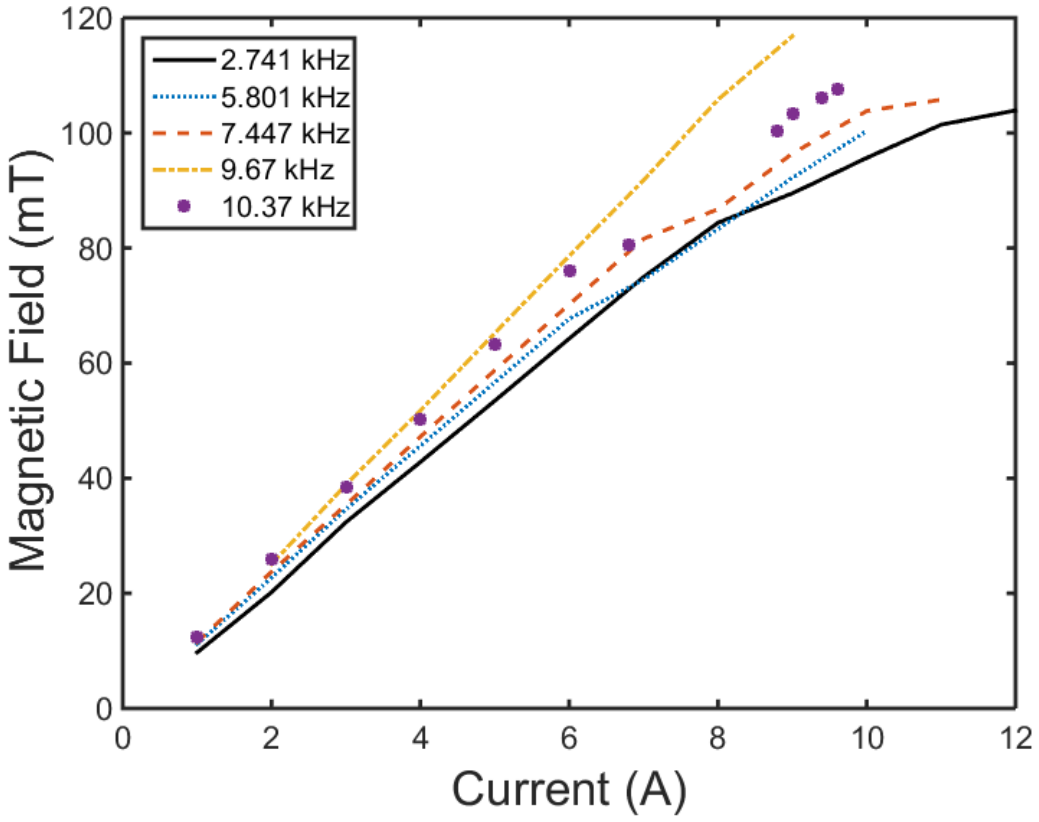

Figure 4.5. Magnetic field versus current when frequency is held constant.

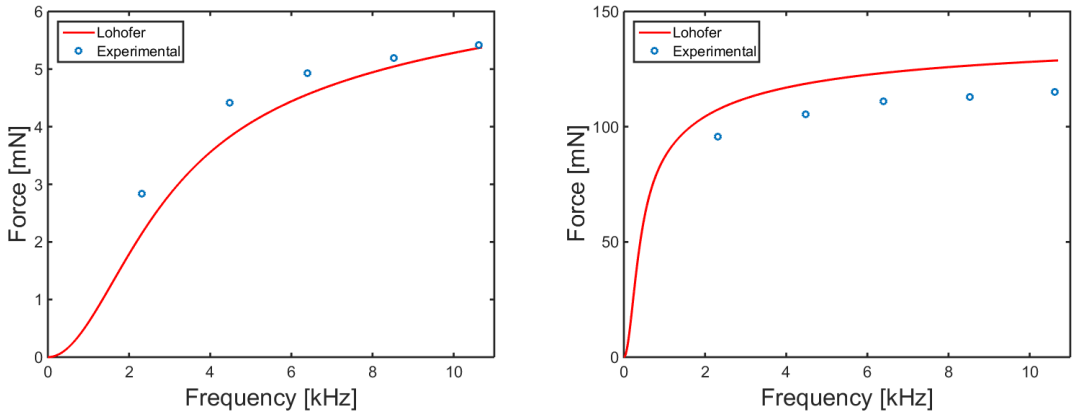

Figure 4.6. Copper sphere force measurement for 5.56 mm diameter (left) and 15.01 mm diameter (right).

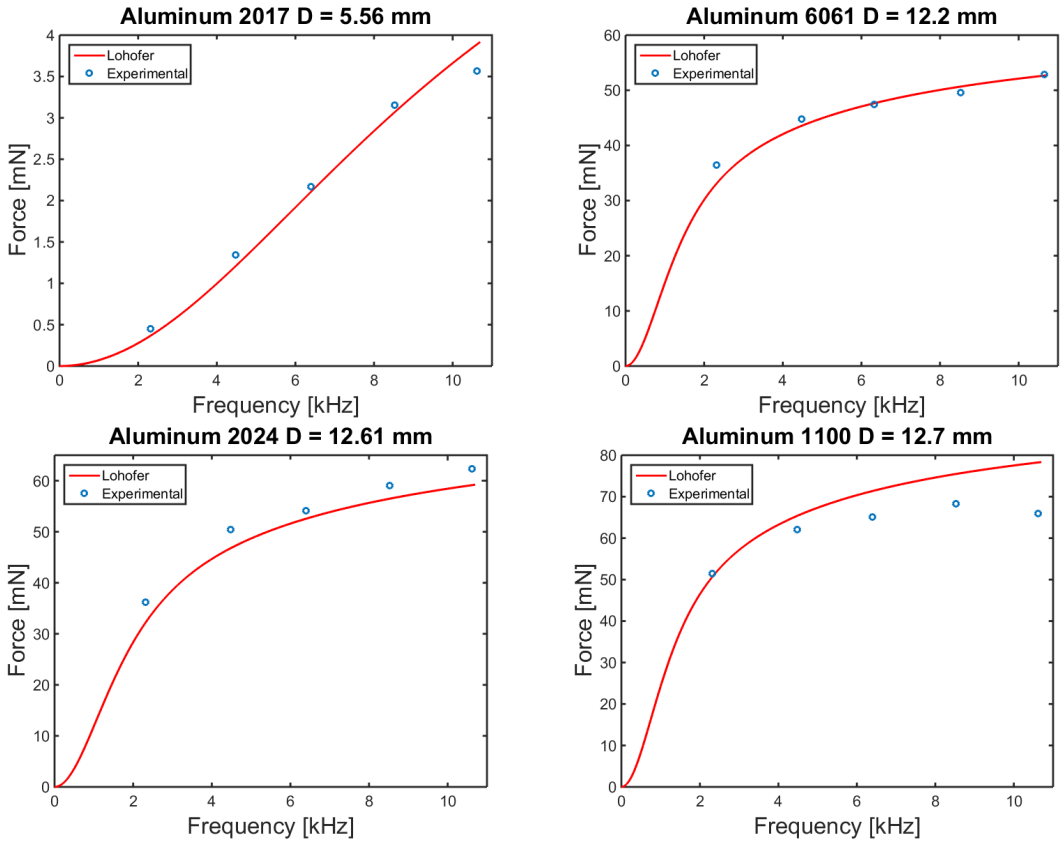

Figure 4.7. Aluminum alloy sphere force measurements.

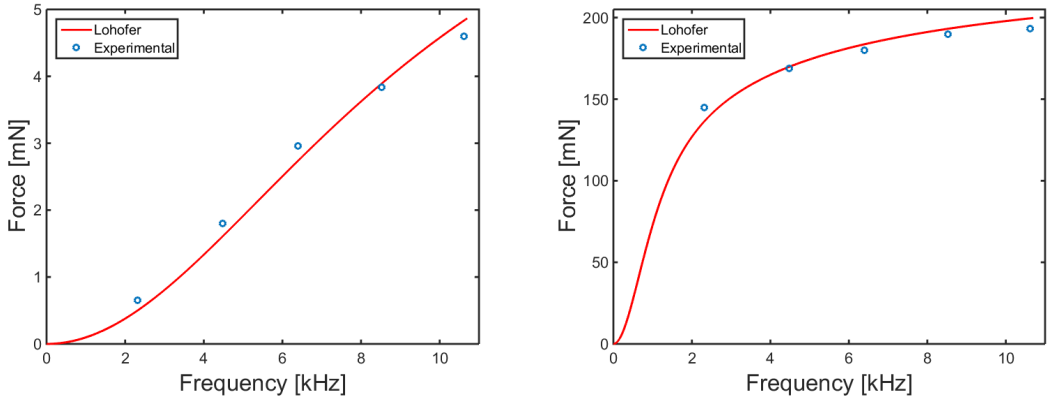

Figure 4.8. Brass sphere force measurements for 6.33 mm diameter (left) and 19 mm diameter (right).

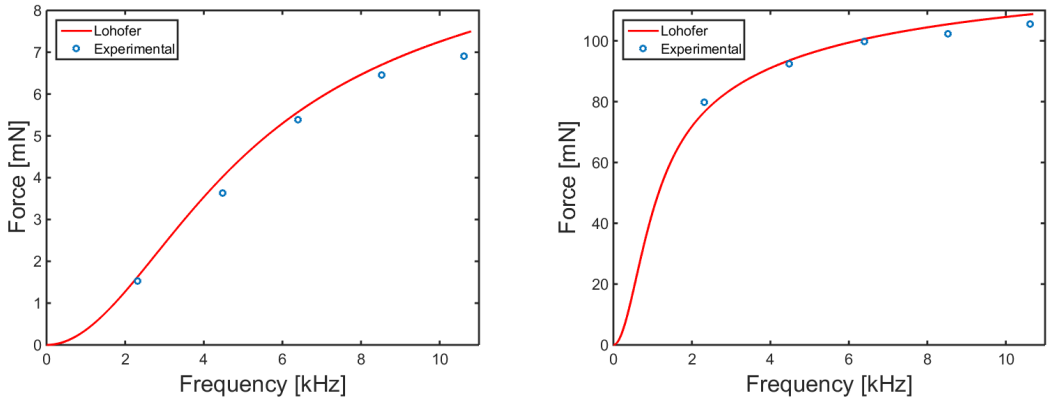

Figure 4.9. Aluminum cylinder force measurements for 6 mm diameter (left) and 12.5 mm diameter (right).

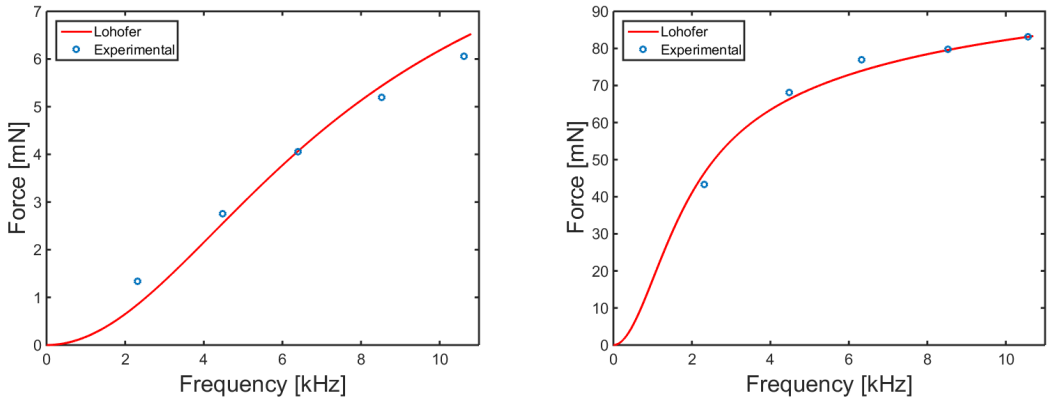

Figure 4.10. Brass cylinder force measurements for 6 mm diameter (left) and 12.5 mm diameter (right).

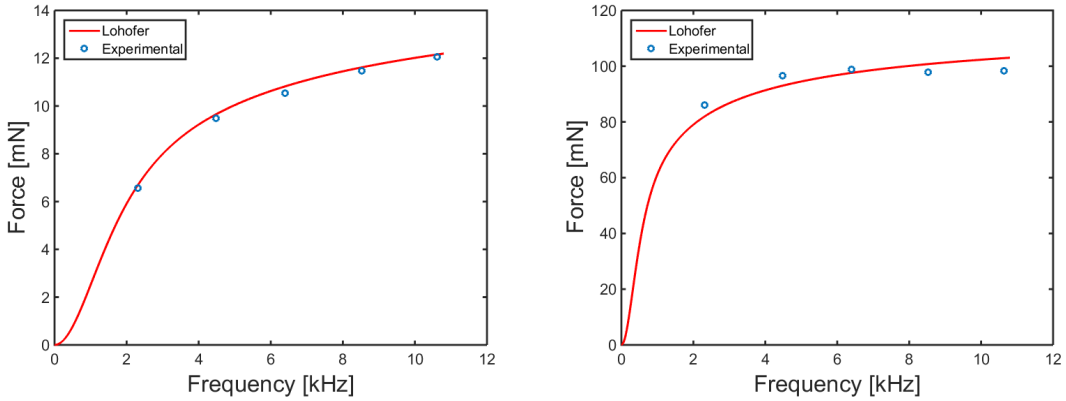

Figure 4.11. Copper cylinder force measurements for 6 mm diameter (left) and 12.5 mm diameter (right).

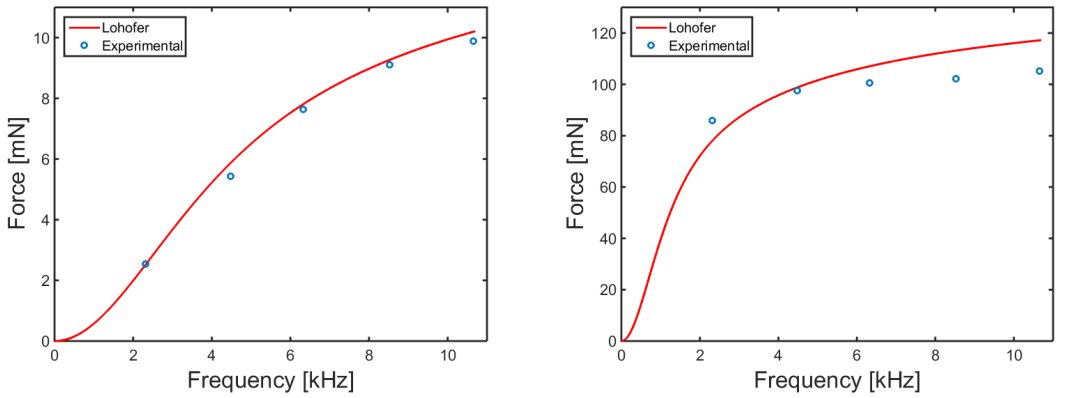

Figure 4.12. Aluminum 6061 cube force measurements for 5.5 mm (left) and 11.4 mm (right).

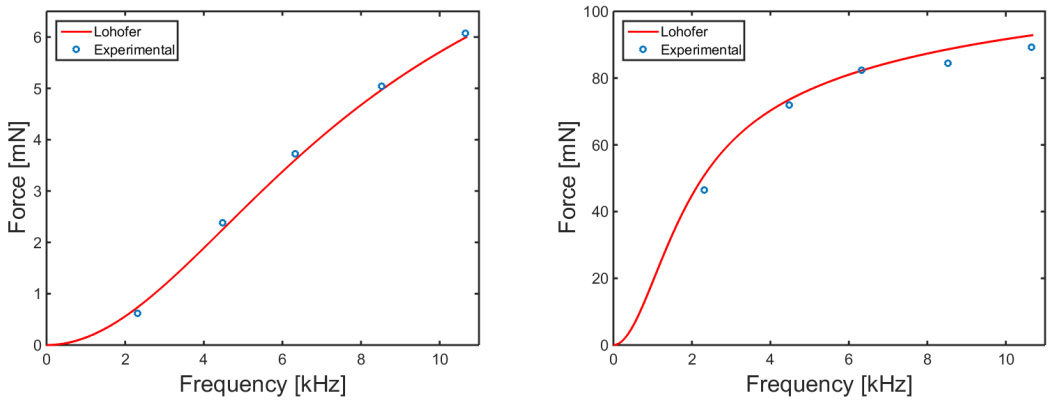

Figure 4.13. Brass cube force measurements for 5.5 mm (left) and 11.4 mm (right).

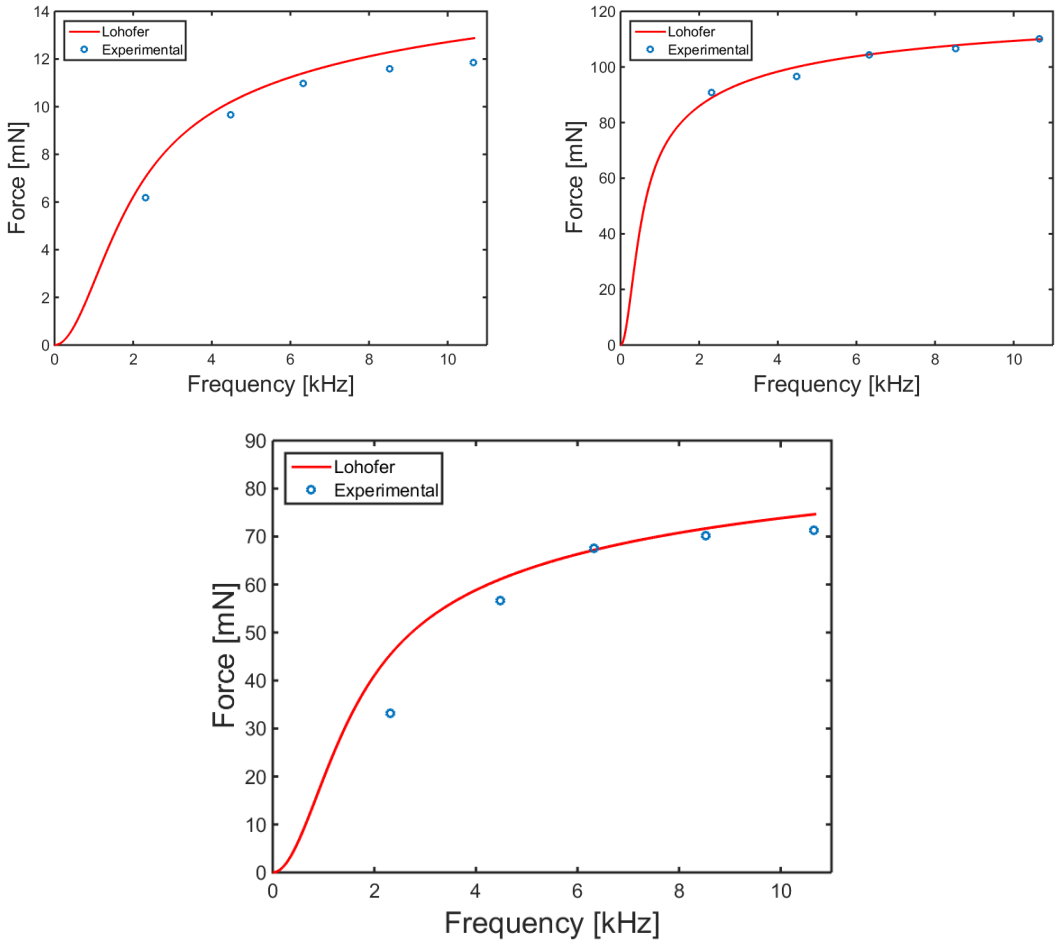

Figure 4.14. Copper cube force measurements for 5.5 mm (left) and 11.4 mm (right). Magnesium cube force measurements for 11.4 mm sample (bottom).

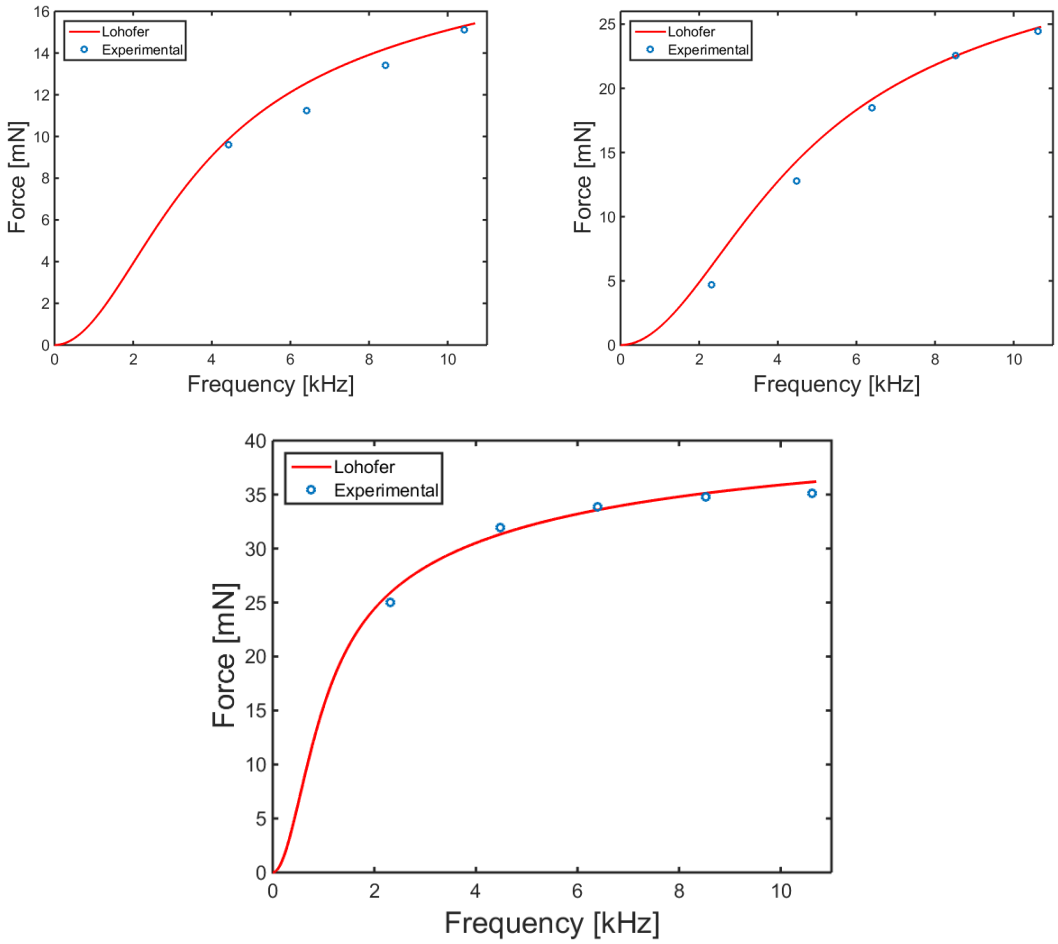

Figure 4.15. Aluminum (left), brass (right), and copper (bottom) disk force measurements.

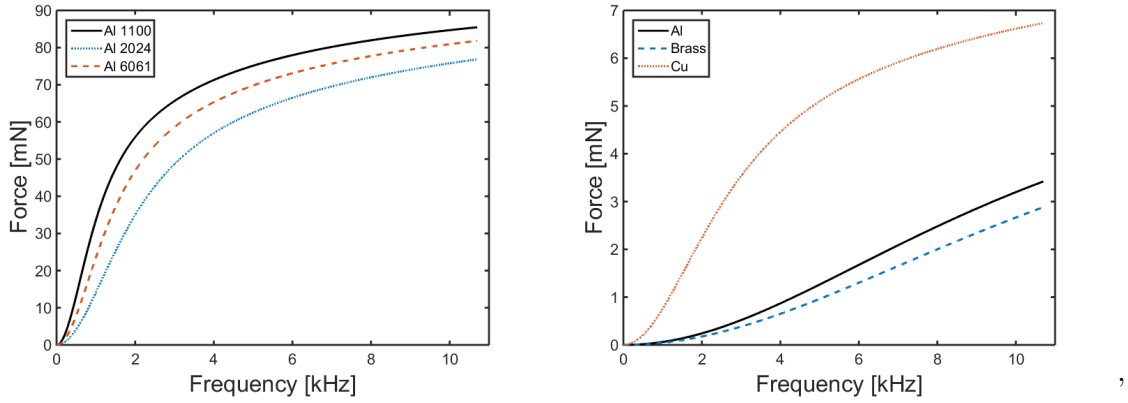

Figure 4.16. Aluminum alloy comparison (left). Aluminum, brass, and copper comparison (right).

CHAPTER 5

CONCLUSION

The principal objective of the work presented in this thesis was to explore the critical properties that constitute EDX technology. Particles that are too small in size or similar in conductivity present a sorting challenge for scrap metal recycling plants. By focusing on these challenges, we have produced an instrument that enhances small particle and alloy sorting abilities by applying the physics governing induced eddy currents.

Mathematical models are an important tool that have been used to improve sorting methods. Surveying the physics has broadened our understanding of the forces involved in EDX. The gap geometry of our toroids was designed to improve the magnetic field strength in the gap, and the gap geometry developed out of our understanding of the physics as they relate to EDX. The most fundamental property of EDX is the magnetic field gradient that produces a force on a particle and induces a torque so as to reject the particle from the field.

Magnetic field strength influences the force a particle experiences and the field is heavily dependent on the type of material out of which the electromagnet is made. As evidenced by Chapter 3, magnetic materials react differently to current and frequency. Chapter 3 showed that a u-shaped magnet made of electrical steel used considerably more power to run than the u-shaped MnZn magnet.

Lohöfer's equation helps us model the behavior of particles with various sizes, shapes, and conductivity. This helped to determine the optimal operating frequency for the magnets. To determine the frequency, Lohöfer's equations were plotted against the measurements of an experiment set up to detect the force felt on objects suspended into a gapped toroid when frequency was varied. The information from that comparison showed that we could used Lohöfer's predictions on nonspherical objects.

EDX makes the recovery of untapped value from particle sizes below 1.0 cm possible.

Shredded nonferrous scrap metal composed mostly of aluminum is known as Zorba. Zorba contains a range of valuable aluminum alloys and is typically sold overseas to be sorted by hand by low-wage workers and where emission regulations are less involved in the smelting process. Smelting Zorba is also energy intensive. Reducing the energy requirements needed to separate aluminum will also reduce emissions and will therefore create a profit for the scrap metal recycle industry in the United States. Under laboratory conditions, EDX has been shown to sort Zorba at 8 to 11 mm in size.

Future explorations involve the development of this technology to sort electronic waste. Electronic waste (e-waste) is defined as any electronic component that has been discarded into municipal waste streams, and is thus ready to be recycled (Kang and Schoenung, 2005). Some examples of e-waste may include televisions, computers, copy/fax machines, and printed circuit boards. Many of these components contain significant amounts of gold, as well as other precious metals, which are desirable for economic recovery.

REFERENCES

Benson, W. H. and T. H. Falconer (1969, June 10). Electrodynamic separator. US Patent 3,448,857.

Edison, T. A. (1890, August 19). Magnetic ore-separator. US Patent 434,588.

Institute of Scrap Recycling (2016, August). Economic impact study U.S.-based scrap recycling industry. `http://www.isri.org/jobs`.

Jackson, J. D. (1998). *Classical Electrodynamics* (Third ed.). Wiley.

Kang, H.-Y. and J. M. Schoenung (2005). Electronic waste recycling: A review of US infrastructure and technology options. *Resources, Conservation and Recycling 45*, 368–400.

Lohöfer, G. (1989, April). Theory of an electromagnetically levitated metal sphere. I. Absorbed power. *SIAM Journal on Applied Mathematics 49*(2), 567–581.

Nagel, J. R. (2016). Induced eddy currents in simple conductive geometries due to a time-varying magnetic field. *IEEE Antennas and Propagation Magazine 58*(??), 10–13. In press (October 2016).

Rony, P. (1964, May 7). The electromagnetic levitation of metals.

Rudenno, V. (2012). *The Mining Valuation Handbook: Mining and Energy Valuation for Investors and Management*. John Wiley & Sons.

Saveliev, V. (1998, June 30). System and method for separating electrically conductive particles. US Patent 5,772,043.